Journal of Drug Delivery Science and Technology 93 (2024) 105409

Contents lists available at ScienceDirect

Journal of Drug Delivery Science and Technology

journal homepage: www.elsevier.com/locate/jddst

Review article

Application of near-infrared light responsive biomaterials for improving the wound healing process: A review

Mariana F.P. Graça [a], André F. Moreira [a,c,**], Ilídio J. Correia [a,b,*]

[a] CICS-UBI - Health Sciences Research Centre, University of Beira Interior, Covilhã, Portugal
[b] CIEPQPF – Departamento de Engenharia Química, Universidade de Coimbra, Rua Silvio Lima, 3030-790, Coimbra, Portugal
[c] CPIRN-UDI/IPG – Center of Potential and Innovation in Natural Resources, Research Unit for Inland Development, Instituto Politécnico da Guarda, Avenida Dr. Francisco de Sá Carneiro, 6300-559, Guarda, Portugal

ARTICLE INFO

Keywords:
Imaging
Near-infrared light
Photobiomodulation
Photodynamic therapy
Photothermal therapy

ABSTRACT

Despite aiming to improve the healing process, the wound dressings that have been developed thus far still present high production costs, uncontrolled drug delivery, and are unable to fully re-establish all features of native skin. In this field, the development of light-responsive dressings has been emerging due to the possibility of controlling the delivery of therapeutic agents both in time and space. Moreover, this strategy has also been explored to guide the materials' polymerization/crosslinking, as well as to mediate therapeutic approaches based on photothermal or photodynamic effects. Among the different approaches, the utilization of near-infrared (NIR) light holds a high translational potential due to the minimal interactions with the biological components and higher penetration capacity in human tissues. In this way, different biomaterials responsive to NIR light have been produced and explored in the production of active wound dressings. Therefore, this review aims to provide an overview of the advantages of NIR light to the wound healing process, in particular, its thermal, photodynamic, photobiomodulation, and imaging potential. Furthermore, the antibacterial, drug-release, and cellular responses that can be obtained with the application of NIR-responsive wound dressings are also described focusing on its impact on the healing process.

1. Introduction

Skin is the largest and outermost organ of the human body and it is enrolled in several functions, namely thermoregulation, prevention of water and fluid loss, immune surveillance, and sensory detection [1,2]. In addition, it also protects the human body against external agents such as microorganisms, ultraviolet (UV) radiation, and mechanical insults [2]. In this way, skin structure and functions may be compromised due to the occurrence of lesions that in some cases exceed its regeneration capacity [3]. So, it is fundamental to develop novel therapeutic approaches that can support and improve the healing process.

In the area of tissue engineering, different wound dressings have been developed, such as sponges, films, hydrogels, and electrospun membranes [2,4–7]. These dressings are non-toxic, biodegradable, and capable of providing a moist environment to the wound site, which improves cell proliferation, migration, and adhesion [8–11]. Furthermore, a wound dressing must facilitate gas and nutrient exchange, while simultaneously protect against bacterial infection [2,12]. Despite these advantages, wound dressings are still associated with high production costs, uncontrolled drug delivery, and the inability to fully re-establish all features of native skin [5].

To address these limitations, researchers have been focused on the development of new bioactive dressings to improve the wound healing process. Among them, the development of light-responsive approaches has been the subject of various studies aiming at controlling the therapeutics' activity both in time and space [13]. For example, irradiation with a light source can be explored to induce a localized polymerization allowing an easy and rapid formation of the polymeric matrix with a high degree of spatial and temporal control, or even the development of *in situ* gelling viscoelastic systems [14]. UV light (<400 nm) is the most applied radiation for mediating the production of wound dressings, namely for triggering hydrogel's reticulation [14]. Additionally, this light source can also be applied for sterilization purposes, treatment of infections, and wound care. Nevertheless, this stimulus may also trigger some adverse effects on mammalian cells, particularly with prolonged or

* Corresponding author. CICS-UBI - Health Sciences Research Centre, University of Beira Interior, Covilhã, Portugal.
** Corresponding author. CICS-UBI - Health Sciences Research Centre, University of Beira Interior, Covilhã, Portugal.
E-mail addresses: afmoreira@fcsaude.ubi.pt (A.F. Moreira), icorreia@ubi.pt (I.J. Correia).

https://doi.org/10.1016/j.jddst.2024.105409
Received 3 August 2023; Received in revised form 13 December 2023; Accepted 22 January 2024
Available online 29 January 2024

Abbreviations

BPQDs - Black phosphorus quantum dots
CCO - Cytochrome C oxidase
CFU - Colony-forming unit
Cip - Ciprofloxacin
CS - Chitosan
E. coli - *Escherichia coli*
h-EGF - Human epidermal growth factor
HIF-1α - Hypoxia-inducible factor 1α
hMSCs - Human mesenchymal stem cells
HSP - Heat shock proteins
ICG - Indocyanine green
NIR - Near-infrared
NIROS - NIR optical scanner
NO - Nitric oxide
P. aeruginosa - *Pseudomonas aeruginosa*
PB - Prussian blue
PBMT - Photobiomodulation
PDA - Polydopamine
PDT - Photodynamic therapy
PTT - Photothermal therapy
ROS - Reactive oxygen species
S. aureus - *Staphylococcus aureus*
UCNPs - Upconversion nanoparticles
UV - Ultraviolet
VEGF - Vascular endothelial growth factor
VLU - Venous leg ulcers

repeated exposure, and present poor penetration in human tissues [15].

In this context, visible light (400–700 nm) has also been explored as an alternative to overcome the toxicity and mutagenic concerns associated with UV light. Despite the potential to trigger the photopolymerization through free radical, ionic, and hybrid approaches or even mediate the activation of photodynamic therapies, visible light still presents a limited penetration in the human body due to its interaction with hemoglobin, cytochromes, and other biomolecules [14–17]. Alternatively, near-infrared (NIR) light emerged as a viable alternative, since it displays minimal interactions with biological components, thus leading to an increased penetration capacity in human tissues. This higher compliance with the human body has been the rationale that triggered researchers to develop biomaterials responsive to NIR light, guiding the materials' polymerization/crosslinking or mediating therapeutic approaches based on photothermal (*i.e.*, light-to-heat conversion) or photodynamic (*i.e.*, light-to-chemical energy; reactive oxygen species (ROS)) effects [18,19]. In the context of photothermal therapy, raising tissue temperature to 41–43 °C can stimulate cell proliferation and angiogenesis. Further temperature increases (*i.e.*, exceeding 50 °C) may be explored to enhance the antibacterial properties of the materials [20–23]. Moreover, the heat generated can also be harnessed to regulate the release of different therapeutic molecules to accelerate and enhance the wound healing process [24]. Similarly, the ROS generation in photodynamic application can also enable the treatment of bacterial infections through oxidative damage or trigger the release of bioactive molecules [24–26]. On the other hand, NIR light can also find application in photobiomodulation (PBMT), in which different biological, chemical, and cellular processes are directly stimulated by the exposition to NIR radiation. Additionally, NIR light also allows the monitoring of the wound healing process through bioimaging approaches [27,28].

With this in mind, this review aims to provide an overview of the NIR light application for accelerating and enhancing the wound healing process. Furthermore, the NIR-responsive biomaterials that can be used to develop wound dressings are also described, focusing on the possible thermal, photodynamic, and photobiomodulating effects and its impact on skin regeneration.

2. Near-infrared light application in biomedicine

Light can interact with different components of the human body, which can result in absorption, scattering, and/or reflection [29]. The NIR light (700–2500 nm) presents a longer wavelength and less energy than the conventionally used visible and UV radiation [30]. Moreover, the main biological components such as blood, skin, and fat present, exhibit lower absorption and scattering coefficients in this region of the spectra [18,31]. Within the NIR light wavelength, three different biological windows (*i.e.*, wavelength regions) were identified: the NIR-I region in the wavelength range of 700–1000 nm; the NIR-II region in the wavelength range of 1000–1350 nm; and the NIR-III region in the wavelength range of 1550–1870 nm [32]. Therefore, the NIR-light responsiveness can be explored as a low-invasive technique to trigger localized treatments and imaging with minimal damage to the surrounding tissues (please see Fig. 1) [29,33,34].

2.1. Photothermal therapy

Photothermal therapy (PTT) is based on the use of photoresponsive agents that mediate the transformation of the NIR light energy into heat. In these approaches, the interaction of the photothermal agent with the NIR radiation results in light absorption and transition to an excited state, followed by energy release via heat generation [18]. Different PTT active agents can be considered to mediate a photothermal effect: inorganic nanomaterials such as those based on gold, iron oxide, copper, and 2D/3D carbon structures (*e.g.*, graphene oxide and carbon nanotubes), organic polymer-based materials (*e.g.*, polydopamine (PDA), polyaniline, and polypyrrole), as well as small molecules (*e.g.*, cyanine-based dyes and prussian blue (PB)) [35–37]. Particularly, inorganic nanomaterials have received significant attention owing to their high photothermal conversion efficiency, facile synthesis/surface modification, as well as adjustable photochemical properties [38,39]. On the other hand, they also possess a lower biocompatibility, when compared to their organic counterparts, poor water dispersibility, and often are nonbiodegradable [36–38]. To overcome the drawbacks of inorganic nanomaterials, different works have been exploring NIR-responsive polymers due to their biodegradability, low toxicity, and photostability [36,37,39]. Nevertheless, these polymers often present a sub-optimal photothermal conversion efficiency and a complicated synthesis process, which limits its biomedical application [37,39]. In turn, small molecules present a good biocompatibility and biodegradability. Nevertheless, this higher biocompliance is counterbalanced by their low photothermal conversion efficiency and poor photostability [18,37].

In wound healing applications, biomaterials such as hydrogels, membranes, and nanofibers can be loaded or combined with these photothermal agents to create a light-triggered therapeutic. For example, Zhang et al. reported that the chitosan (CS) -based aerogel with amino-functionalized molybdenum disulfide nanosheets have a photothermal conversion efficiency of 37.9 % and could reach a maximum temperature of 60 °C under the NIR laser irradiation (808 nm, 2 W/cm^2, 10 min) [40]. Similarly, Tao et al. developed a hydrogel composed of dibenzaldehyde-grafted poly (ethylene glycol) and lauric acid-terminated CS and loaded with curcumin-loaded mesoporous PDA nanoparticles [41]. The photothermal studies demonstrated that the hydrogels could mediate a temperature increase up to 59.3 °C under NIR irradiation (808 nm, 1 W/cm^2, 10 min), corresponding to a photothermal conversion efficiency of 23.93 %. In the same way, Zhou et al.

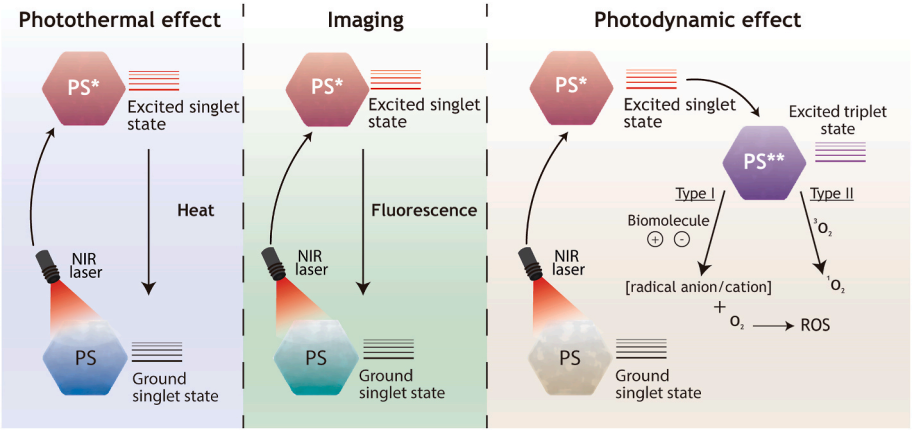

Fig. 1. Illustration of the mechanisms behind the PTT, imaging, and PDT that can be triggered by photoresponsive agents in response to NIR irradiation.

reached a temperature of ≈65.2 °C upon NIR irradiation (808 nm, 1.5 W/cm^2, 10 min) of an electrospun membrane based on poly (lactic-*co*-glycolic acid) containing MXene/Ag_2S bio-heterojunctions and lactate oxidase [42].

2.2. Photodynamic therapy

Photodynamic therapy (PDT) is based on the conversion of light energy in singlet oxygen and other ROS by the action of a photosensitizer [43]. Such occurs due to the transition of the photosensitizer to an excited state (excited triplet state) upon interaction with the light, which can undergo two different reactions. In type 1 reactions, the photosensitizer interacts directly with the cell membrane, molecules, or other substrates to form a radical anion or cation depending on the transfer of a proton or an electron, respectively. These intermediaries may also react with oxygen promoting the formation of ROS [24,43]. Otherwise, in type 2 reactions, the excited photosensitizer interacts directly with molecular oxygen originating singlet oxygen [24]. Until today, different photosensitizers have been explored to mediate the formation of ROS such as polymers containing selenium or tellurium, poly (propylene sulfide), vinyl ether/disulfide, nanomaterials (*e.g.*, gold, silver, graphene oxide and upconversion nanoparticles (UCNPs)), and small molecules (*e.g.*, cyanines, tetraphenylchlorin or boron dipyrromethene) [24,26,44,45]. Sun et al. developed an electrospun membrane enriched with UCNPs and porphyrinic metal-organic frameworks for application in PDT and in wound healing [46]. The authors observed that with the irradiation with a NIR laser (980 nm, 0.5 W, 30 min), the 1,3-diphenylisobenzofuran (ROS indicator) relative absorbance decreased ≈ 30 % indicating the generation of ROS, in contrast, no significant alterations were observed in the absence of NIR light. Similarly, Du et al. produced a 3-(trimethoxylmethosilyl) propyl methacrylate hydrogel incorporating Ag_2S quantum dots coated with mesoporous silica for treating bacterial wound infections [47]. The *in vitro* studies revealed that upon NIR irradiation (808 nm, 1.8 W/cm^2, 4 min), the hydrogel-treated groups present a stronger dichlorofluorescein diacetate fluorescence, which is indicative of higher ROS generation [47].

2.3. Imaging

The lower absorption and scattering coefficients of the biological components to NIR light support the development of novel light-based imaging techniques using these wavelengths [28,48]. For that purpose, researchers have been developing non-contact NIR imaging devices or fluorescent agents that can be excited and emit light in the NIR region. In the latter, fluorescent dyes such as cyanine-based dyes (indocyanine green (ICG), IR780, and IR825), PB, and Ag_2S quantum dots can be used to allow the *in vivo* imaging [49–51]. Among them, ICG and PB are already approved by the Food and Drug Administration for different human applications [52,53]. Chen et al. used Ag_2S quantum dots to label human mesenchymal stem cells (hMSCs), which allowed the detection of the hMSCs' migration to the wound site and colonization of the collagen scaffolds, via NIR-II fluorescence imaging [51]. In turn, Mai et al. developed a new pH-sensitive NIR fluorescent probe (AlkaP-1), based on a modified IR-780 molecule, to monitor the progress of the healing process in chronic wounds [49]. The authors observed a significant reduction in the fluorescence signal (*i.e.*, emission at 790 nm) with the increase in the pH value from 4.5 to 10.5. Moreover, the probe also allowed to monitor the alkalization as well as the heterogeneity of pH within the wound bed during the development of chronic wounds [49].

3. Application of NIR light in skin regeneration

The application of NIR light has emerged in recent years as a promising and straightforward strategy for enhancing the wound healing process. In the following sections, the various applications of NIR light for enhancing skin regeneration will be summarized, focusing on the PTT and PDT potential for mediating antibacterial effects, promoting mild-hyperthermy, or even controlling drug delivery. Moreover, the PBMT or low-level laser therapy and the NIR imaging potential will also be described. The different applications of the NIR light in the wound healing process are illustrated in Fig. 2.

3.1. Photothermal effect for enhancing wound healing

The generation of heat by the photothermal agents is dependent on the laser parameters (*e.g.*, irradiation wavelength, time, and power) as well as the materials' absorption capacity and light-to-heat conversion efficiency (already described in detail elsewhere [54–56]). In the following sections, various impacts of light-mediated heat generation on the wound healing process will be elucidated, with a focus on antibacterial effects, biological enhancement, and controlled release approaches.

3.1.1. Antibacterial properties

Bacterial infections are among the most common complications occurring during skin injuries, significantly impacting the wound healing process. The bacterial endotoxin and exotoxin, tissue-destroying enzymes, and antiphagocytic capacity disrupt normal physiological processes and difficult the achievement of hemostasis [57]. Moreover, their presence also prolongs the inflammation phase, resulting in high levels of pro-inflammatory cytokines and increased production of matrix metalloproteinases [57]. The over-colonization of pathogens also retard

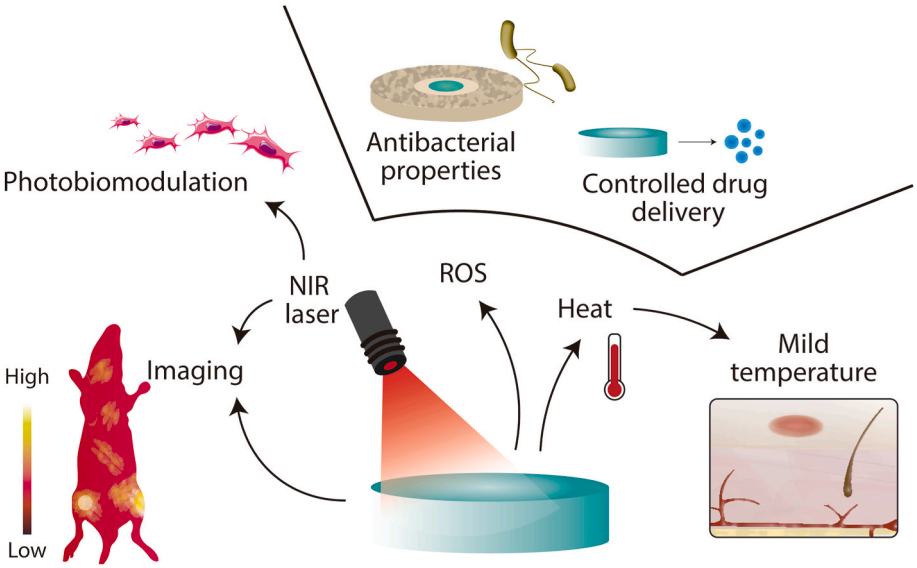

Fig. 2. Illustration of the different effects that can be activated by NIR light and explored in wound healing applications.

the proliferative phase and re-epithelization, reducing the expression of the endothelial growth factor receptor as well as suppressing endothelial cells' migration and proliferation [57,58]. Additionally, local infections may progress to systemic infections, posing a threat to the patients' life [58]. Taking this into consideration and the increasingly widespread bacterial resistance to antibiotics, researchers have been developing novel strategies to prevent and fight infections.

The localized increase of temperature to values superior to 48 °C can induce the membranes' rupture, enzyme inactivation, and proteins' denaturation [18]. Therefore, the photothermal effect can induce damage to the bacteria's structural elements, disrupt the bacterial cell wall, and even trigger bacterial death [18,59]. Moreover, the PTT should have a broad-spectrum efficacy, and no significant side effects or development of bacterial resistance mechanisms are expected to occur [60]. In Table 1 it is provided an overview of the NIR-responsive biomaterials aimed for antibacterial applications in skin regeneration, describing the irradiation parameters, its effect, and the major results.

For this purpose, one of the most explored approaches is based on the utilization of nanoparticles as photothermal agents for mediating the localized temperature increase [7,62,70]. For example, Chen et al. produced polycaprolactone and gelatin electrospun fibers loaded with a nanoagent composed of zeolitic imidazolate framework-8, ciprofloxacin hydrochloride, and sodium polyacrylate (PCL/Gel/ZCPC) for application in the wound healing process and protection against bacterial infection [62]. The authors observed that the wound dressing could mediate a temperature increase to 40.4 °C, 48.3 °C, and 64 °C when the power density of the NIR laser irradiation (808 nm, 10 min) increased from 0.33 W/cm^2, 0.5 W/cm^2, to 1 W/cm^2, respectively. Moreover, when incubated with *Escherichia coli* (*E. coli*), the antibacterial effect PCL/Gel/ZCP fibers provoked a 30 %, 70 %, and 83 % reduction in the colony-forming unit (CFU)/mL when irradiated with a NIR laser (808 nm, 0.5 W/cm^2) for 10, 20, and 30 min, respectively. In turn, for the *Staphylococcus aureus* (*S. aureus*) group, these values were slightly higher with a 10 %, 63 %, and 83 % reduction in the CFU/mL. Furthermore, the *in vivo* assays performed in *S. aureus* infected wounds revealed that at day 14, the wound healing ratio for the PCL/Gel/ZCPC fibers + laser group was 98.7 %, while for the Tegaderm™, PCL/Gel fibers, and PCL/Gel/ZCPC fibers were 81.7 %, 88.3 %, and 91 %, respectively. The wounds treated with PCL/Gel/ZCPC fibers, under NIR laser irradiation, had a greater wound healing effect with less inflammatory cells as well as significantly higher neovascularization and collagen regeneration, comparatively with the other groups [62].

Similarly, Zhang et al. incorporated dopamine-modified gelatin@Ag nanoparticles into guar gum hydrogel (Gel-DA/GG@Ag) for application in tissue repair and wound healing with a NIR-activated antibacterial activity [7]. The authors observed that the temperature reached upon the hydrogels irradiation with a NIR laser (808 nm, 2 w/cm^2, 10 min) increased with the concentration of $AgNO_3$, 0.5, 1, and 2 mg/mL, reaching ≈ 47.6 °C, ≈52.0 °C and ≈55.4 °C, respectively. Furthermore, the NIR irradiation (808 nm, 2 W/cm^2, 10 min) enhanced the antibacterial efficacy against *S. aureus* from ≈72 % to 96.88 % and *E. coli* from ≈52 % to 98.96 %. The *in vivo* studies performed in *S. aureus* infected wounds showed that the combination of the hydrogel administration plus NIR irradiation led to almost complete wound closure (99.9 %) in 10 days, without any signs of bacterial infection [7].

3.1.2. Mild-hyperthermia

Apart from the antibacterial potential of the localized heat generation, milder temperatures (below 48 °C) can have a positive impact on the cell's proliferation, angiogenesis, and tissue repair [19,71]. Moreover, different studies correlated the increased expression of heat shock proteins (HSP) with the mild-hyperthermy treatments [19,72]. This family of proteins is responsible for recruiting cells, promoting cell migration, and consequently accelerating wound healing [72,73]. Furthermore, HSP's also play an important role in the repair of potential cellular damages that can occur when cells are subjected to temperatures higher than 37 °C [19,72]. Additionally, milder temperatures can also increase blood flow, modulate the activity of enzymes, activate cell signaling pathways, and still present antibacterial capacity [72,74,75]. Table 2 provides an overview of the NIR-responsive biomaterials applied in mild-hyperthermy treatments for skin regeneration.

Chen et al. developed a piezoelectric and photothermal CS film coated with PDA to enhance the wound healing process [72]. The authors observed that the wound dressing could promote the local increase of the temperature to ≈45 °C after NIR irradiation (808 nm, 0.7 W/cm^2, 9 min) *in vivo*. Moreover, on day 7, the mice treated with the *C*S-PDA film and NIR presented a wound closure of 82.2 ± 2.7 %, whereas the mice treated only with the *C*S-PDA film, CS plus NIR, and CS presented lower wound closures, 73.3 ± 1.7 %, 67.3 ± 6.0 %, 61.7 ± 3.9 %, respectively. The authors correlated the enhanced wound healing process with the upregulation of Ki67 (a cell proliferation marker) and Bcl-2 (an anti-apoptotic protein), increased expression of HSP 90, HIF-1α, and vascular endothelial growth factor (VEGF) [72]. In turn, Dong et al. analyzed the effects of the mild temperature promoted by NIR

Table 1
NIR-responsive biomaterials with antibacterial properties for application in the wound healing process. Note: The results refer to data obtained in the *in vivo* assays.

Biomaterial	Composition	Photo-triggered effect			Results	Ref
			Irradiation Parameters	Effect		
Membranes	Electrospun membrane of poly (lactic-*co*-glycolic acid), MXene/Ag2S bio-heterojunctions, and lactate oxidase (*P*-MX/AS@Lox)	PDT and PTT	808 nm 1.5 W/cm^2 10 min	ΔT = 38.7 °C; Continual fluorescence decay of DPBF in the case of *P*-MX/AS@Lox + Laser, while the absorption has no remarkable attenuation in the other group.	After treatment with *P*-MX/AS@LOx + NIR, the bacterial survival rates for *S. aureus* and *E. coli* were ≈0 %.The wounds treated with *P*-MX/AS@LOx membranes + NIR presented a better wound healing process, lower expression of inflammatory factors, achieved hemostasis, enhanced collagen deposition, and angiogenesis.	[42]
	Nanofibers based on polycaprolactone, polyvinylpyrrolidone, and UCNPs	PDT	808 nm 0.5 W/cm^2 20 min	The concentration of singlet oxygen gradually increases with the irradiation time and doping concentration of UCNPs, until 20 min of irradiation and 0.20 wt%.	3 days after treatment, the PDT group showed a bacterial survival rate of ≈0.0 % in the Methicillin-resistant *S. aureus*-infected wounds. Wounds treated with PDT healed faster than other groups (16 days instead of 24 days) and demonstrated reduced inflammation and promotion of collagen regeneration.	[61]
	Polycaprolactone/gelatin fibers incorporating a nanoagent (2.5 mg/mL) based on zeolitic imidazolate framework-8, ciprofloxacin hydrochloride, and sodium polyacrylate (PCL/Gel/ZCPC)	PTT	808 nm 0.5 W/cm^2 10 min	ΔT = 16.3 °C	PCL/Gel/ZCPC fibers + NIR treated groups showed ≥99 % reduction in the number of colonies of *S. aureus* and *E. coli*. After 14 days, PCL/Gel/ZCPC fibers + NIR treated wounds presented a wound healing ratio of 98.7 %, fewer inflammatory cells, higher neovascularization and collagen regeneration, contrasting with wound healing ratio of 81.7 %, 88.3 %, and 91 % for Tegaderm™, PCL/Gel fibers, and PCL/Gel/ZCPC fibers.	[62]
Nanostructure	Quaternized Cu-carbon dots (Cu-RCDs-C35)	PDT and PTT	808 nm 2 W/cm^2 5 min	ΔT = 19.2 °C; The absorbance intensity of DPBF gradually decreases after treatment with Cu-RCDs-C35 plus Laser.	Cu-RCDs-C35 dots + NIR showed an antibacterial efficacy against *E. coli* and *S. aureus* of 99.36 % and 99.98 %, while without NIR this value decreased to 62 % and 66 %, respectively. Cu-RCDs-C35 + NIR treated wounds showed a healing ratio of 96 % (with the lowest number of bacterial colonies and enhanced collagen deposition), while this value was smaller for PBS + NIR, Cu-RCDs, and RCDs-C35 + NIR groups, *i.e.*, 62 %, 70 %, and 85 %, respectively.	[63]
	Copper ions-hydroxyapatite/polydopamine nanocomposites (HA-Cu/PDA)	PDT and PTT	808 nm 1 W/cm^2 10 min	ΔT = ≈ 21 °C. The HA-Cu/PDA plus NIR treatment exhibited a higher level of ROS (≈3 and ≈5.2) against *E. coli* and *S. aureus* than without NIR irradiation (≈1.3 and ≈1.6).	HA-Cu/PDA + NIR showed an antibacterial efficacy against *E. coli* and *S. aureus* of 91.0 % and 93.2 %. After 14 days, HA-Cu/PDA + NIR treated wounds showed a closure of ≈98 % with reduced inflammatory response and enhanced collagen deposition and angiogenesis, while the control, HA, HA + NIR, and HA-Cu/PDA groups showed a wound closure of ≈66 %, ≈79 %, ≈81 %, and ≈84 %.	[64]
	Polypyrrole - bismuth oxychloride intercalated nanosheets (PPy-BiOCl)	PDT and PTT	808 nm 1 W/cm^2 10 min	ΔT = 20 °C The intercalated nanosheets presented the highest fluorescence intensity, which was indicative of ROS production.	PPy-BiOCl + NIR showed an antibacterial efficacy against *S. aureus* and *E. coli* of 99.25 % and 99.23 %, respectively, contrasting with the 10.02 % and 9.87 % for BiOCl and 33.84 % and 33.86 % for PPy, respectively. PPy-BiOCl + NIR treated wounds presented no bacterial infection, inhibition of the inflammatory response, and increased collagen deposition.	[65]
	Nanosystem based on PB, PDA, and Ag	PDT and PTT	808 nm	T = 53 °C Only the groups with NIR irradiation demonstrated the capacity for ROS production.	PB@PDA@Ag + NIR presented an antibacterial efficacy against Methicillin-resistant *S. aureus* and Ampr	[66]

(*continued on next page*)

Table 1 (*continued*)

Biomaterial	Composition	Photo-triggered effect			Results	Ref
			Irradiation Parameters	Effect		
			1 W/cm^2		*E. coli* of ≈99.99 % and ≈99.77 %, respectively. After 8 days with PB@PDA@Ag + NIR, the area of infected wounds was 22.79 %, with antibacterial capacity, lower inflammatory response, and up-regulation of VEGF expression, while with PBS, NIR, PB, PB + NIR, PB@PDA, PB@PDA + NIR, and PB@PDA@Ag groups showed higher wound areas, 58.79 %, 59.24 %, 56.81 %, 47.90 %, 51.46 %, 41.77 %, and 41.88 %, respectively. 5 min	
Hydrogels	Hydrogel composed of ε-Polylysine, PDA, and agarose	PTT	808 nm 1 W/cm^2 10 min	ΔT = ≈ 27.4 °C	The hydrogel + NIR treatment decreased the number of colonies of *S. aureus* and *E. coli* by ≥ 70 % after 5 min, and 100 % after 10 min. Hydrogel + NIR treated wounds presented a lower number of bacteria, reduced inflammation, accelerated collagen deposition, and improved vascularization.	[67]
	Dopamine-modified gelatin@Ag nanoparticles incorporated into guar gum hydrogel	PTT	808 nm 2 W/cm^2 3 min	ΔT = 21.2 °C	After treatment with hydrogel + NIR, the antibacterial efficacy against *S. aureus* and *E. coli* increased from ≈72 % to ≈52 %–96.88 % and 98.96 %, respectively. After 10 days of treatment with Gel-DA/GG@Ag1 + NIR, the wounds presented a healing ratio of 99.9 %, contrasting with the ≈90 %, ≈95 %, ≈98 %, and 98.6 % registered for control, GG, Gel-DA/GG, and Gel-DA/GG@Ag1, respectively.	[7]
	Germanene-modified CS hydrogel	PTT	808 nm 2 W/cm^2 5 min	ΔT = 23.2 °C	After treatment with the hydrogel + NIR, the antibacterial efficacy against *E. coli* and *S. aureus* increased from ≈9 % to ≈14 %–98.76 % and 99.81 %, respectively. After 12 days of treatment with CS/Ge NCs0.8 hydrogel + NIR, the wound presented a relative area of ≈0 % with a lower number of bacterial colonies, while with PBS, CS/Ge NCs0 hydrogel and CS/Ge NCs0.8 hydrogel presented a wound area of ≈22 %, ≈12 %, and ≈10 %, respectively.	[68]
	Ag_2S quantum dots-mesoporous silica (420 μg/mL) incorporated into 3-(trimethoxylmethosilyl) propyl methacrylate hydrogel	PDT and PTT	808 nm 1.8 W/cm^2 1 min	ΔT = 27.1 °C the hydrogel + NIR group displayed stronger ROS fluorescent signals.	After treatment with the hydrogel + NIR, the number of colonies of *E. coli* and Methicillin-resistant *S. aureus* decreased to 99.7 % and 99.8 %, respectively. Hydrogel + NIR enhanced the wound healing process with lower expression of IL-6 and higher expression of VEGF, without any significant vantages in the antibacterial efficacy.	[47]
	α-lipoic acid modified palladium nanoparticles incorporated into sodium alginate hydrogel	PTT	808 nm 2 W/cm^2	ΔT = 35.1 °C (5 min of irradiation)	After treatment with hydrogel + NIR, the antibacterial efficacy against *E. coli* and *S. aureus* increased from 10 % to >80 %. After 15 days of treatment with hydrogel + NIR, the wounds had a relative area of ≈1 % with the lower number of *S. aureus* colonies, while the control, sodium alginate, and hydrogel	[69]

(*continued on next page*)

Table 1 (*continued*)

Biomaterial	Composition	Photo-triggered effect		Results	Ref
		Irradiation Parameters	Effect		
		10 min		groups had relative area of ≈16 %, ≈11 %, and ≈10 %, respectively.	

Table 2
NIR-responsive biomaterials used on mild-hyperthermy treatments for skin regeneration. Note: The results refer to data obtained in *vivo* assays. (N.A.: Not Available).

Biomaterial	Composition	Irradiation Parameters	Temperature (°C)	Result	Ref
Hydrogel	Polyacrylamide hydrogels incorporating Cs_xWO_3 nanorods (2.0 mg/mL)	980 nm 2.5 W/cm^2 15 min	43.7	After 10 days of treatment with the hydrogel + NIR, the wounds presented a wound area of 4.4 %, with enhanced re-epithelization, formation of granulation tissue, and collagen deposition, while the hydrogel and NIR groups had wound areas of 19.0 ± 0.7 % and 14.1 ± 2.1 %, respectively.	[76]
	Hydrogel based on fayalite (0.5 w/v %) and N, *O*-carboxymethyl CS.	808 nm 0.36 W/cm^2 15 min	40	After 14 days of treatment with the hydrogel + NIR, the wounds presented enhanced angiogenesis and wound closure of ≈100 %, contrasting with the ≈78 % of the single treatment with the hydrogel.	[20]
	Polyethyleneimine-graphene oxide (6 mg/mL), carboxymethylated CS, and aldehyde-polyethylene glycol hydrogel (GCP hydrogel)	808 nm 2 W/cm^2 5 min	41–44	After treatment with GCP + NIR, the wound was completely closed and showed an enhanced collagen deposition, re-epithelialization, and angiogenesis, while the control, NIR, and GCP groups presented a wound area of 21.6 %, 20.7 %, and 14.1 %, respectively.	[21]
	Niobium carbide (40 μg/mL) based hydrogel with PLGA-PEG-PLGA (Nb_2C@Gel)	808 nm 1.5 W/cm^2 10 min	48	After treatment with the Nb_2C@Gel + NIR, the wound presented a bacterial survival rate of ≈5 %, with lower inflammatory response and oxidative stress, and enhanced angiogenesis and tissue regeneration. Control, Gel, and Nb_2C@Gel treated groups had bacterial survival rates of ≈100 %, ≈99 %, and ≈38 %, respectively.	[77]
Cryogel	CS and silk fibroin cryogel incorporating PDA nanoparticles (6.4 wt %)	808 nm 2 W/cm^2 30 min	45	The treatment with cryogel + NIR improved skin tissue regeneration, with the wound closure increasing from ≈93 % to ≈99 % at day 21.	[34]
Film	CS film coated with PDA (8 mg/mL)	808 nm 0.7 W/cm^2 9 min	45	After 7 days of treatment with *C*S-PDA film + NIR, the wounds presented a wound closure of 82.2 %, including promotion of cell proliferation, migration, angiogenesis, and collagen deposition. The *C*S-PDA film, CS + NIR, and CS treated groups presented a wound closure of 73.3 %, 67.3 %, and 61.7 %, respectively.	[72]
Nanostructure	Antimicrobial peptides-Au/Ag nanorods (20 μM)	808 nm 0.8 W/cm^2 40–60 s	< 47	After treatment with nanorods + H_2O_2 + NIR, the wound presented ≈ 89 Methicillin-resistant *S. aureus* CFU and a 94.9 % decrease in the wound area, while without NIR a lower efficacy was registered, ≈46,773 CFU and wound area of 62.8 %.	[74]
	Molybdenum disulfide nanoflakes modified with quaternized CS (1 mg/mL)	808 nm 1.25 W/cm^2 5 min	45	The treatment with QCS-MoS2-OFLX + NIR, decreased the CFU/mL of Methicillin-resistant *S. aureus* to ≈15 %, while the QCS-MoS_2, OFLX and QCS-MoS_2-OFLX treated groups had a lower efficacy, ≈98 %, ≈71 % and ≈70 %, respectively.	[75]
	Silica nanosphere with copper sulfide nanoparticles and cinnamaldehyde (SiO2@CA@CuS, 400 μg/mL)	980 nm 1 W/cm^2 5 min	45	After 7 days of treatment with SiO_2@CA@CuS nanoplatform + NIR, the *S. aureus*-infected wound presented an accelerated healing process without registering signs of toxicity in major organs.	[78]
Particles	Porous silicon with the surface modified with PDA-Cu, incorporating curcumin	808 nm 0.33 W/cm^2 5 min	45	After 7 days of treatment with CuPPSi + NIR, the wound presented a wound area of 27.8 % with fewer colonies of bacteria, increased re-epithelialization and collagen maturation, while in PBS, PBS + NIR, and CuPPSi groups the wound area was 61.3 %, 62.3 %, and 35.2 % respectively.	[79]
Asymmetric wound dressing	PNIPAAm hydrogel loaded with CuS nanoparticles with CS/polyvinyl alcohol nanofiber membrane (PNIPAAm-PVA/CS-CuS)	808 nm N.A. 30 min	40 (*in vitro*, 808 nm, 1 W/cm^2, 22 min)	After 17 days of treatment with PNIPAAm-PVA/CS-CuS + NIR, the wound presented a healing rate of 89.33 %, larger number of collagen fibers, epidermal structure, and granulation tissue, while in PVA/CS hydrogels-PVA/CS-CuS + NIR, PNIPAAm-PVA/CS-CuS, PVA/CS and sterile gauze treated groups the wound healing rate was 70.67 %, 56.25 %, 62.50 %, and 50 %, respectively.	[22]

irradiation with antimicrobial peptides (Dap)@Au/Ag nanorods to treat drug-resistant bacterial infections [74]. The NIR laser irradiation (808 nm, 0.8 W/cm^2, 40–60 s) of Methicillin-resistant *S. aureus* infected wounds and treatment with the nanorods promoted a temperature increase at the body surface up to 47 °C. This photothermal treatment led to the reduction of the Methicillin-resistant *S. aureus* bacteria viability, *i.*

e., the group treated with nanorods plus H_2O_2 presented ≈46,773 CFU while with the additional NIR irradiation (808 nm, 0.8 W/cm^2, 40–60 s) this value decreased to ≈ 89 CFU. Moreover, the mild-hyperthermy also improved wound contraction, reaching a 62.8 % decrease in the wound area for Dap@Au/Ag nanorods (+H_2O_2) group, while under NIR irradiation this value reached the 94.9 % (Fig. 3) [74].

3.1.3. Drug delivery

The NIR light can also be explored to trigger and control the drug release in wound healing applications, mainly through the photothermal effect. In that approach, thermoresponsive biomaterials react to the heat generated upon irradiation with a NIR laser, allowing the release of the therapeutic molecules [24]. Table 3 presents examples of NIR-responsive biomaterials applied in the wound healing process with a light-triggered drug release.

For example, Zhang et al. produced microparticles based on different natural polymers (*e.g.*, silk fibroin, gelatin, agarose) and loaded with black phosphorus quantum dots (BPQDs) for mediating the delivery of growth factors and antibacterial peptides in wound healing applications [85]. The BPQDs act as photothermal agents and the temperature increase in response to the NIR laser irradiation will be explored to trigger the release of the bioactive molecules in a process controlled by the melting of the gelatin. The authors reported that the microparticles (0.2 mg/mL of BPQDs) could mediate the increase in the media temperature up to 40 °C with the NIR laser irradiation (808 nm, 2.41 W/cm^2, 1 min). Moreover, the heat generation under NIR laser irradiation accelerated the drug release reaching 46 % at 10 h and after 20 irradiation cycles, whereas the non-irradiated microspheres released less than 20 % of loaded bovine serum albumin. In turn, the study performed in *E. coli*-infected full-thickness wounds revealed almost complete wound healing in the microparticles plus NIR-treated group, showing improved granulation tissue formation, re-epithelization, collagen deposition, and angiogenesis. Additionally, this treatment also avoided the establishment of bacterial infection at the wound site [85]. The localized temperature increase can also promote the sol-gel conversion of the hydrogels and therefore control the drug release [86]. Liu et al. developed a temperature-sensitive hydrogel containing mesoporous PDA@-ciprofloxacin (MPDA@Cip) nanoparticles and human epidermal growth

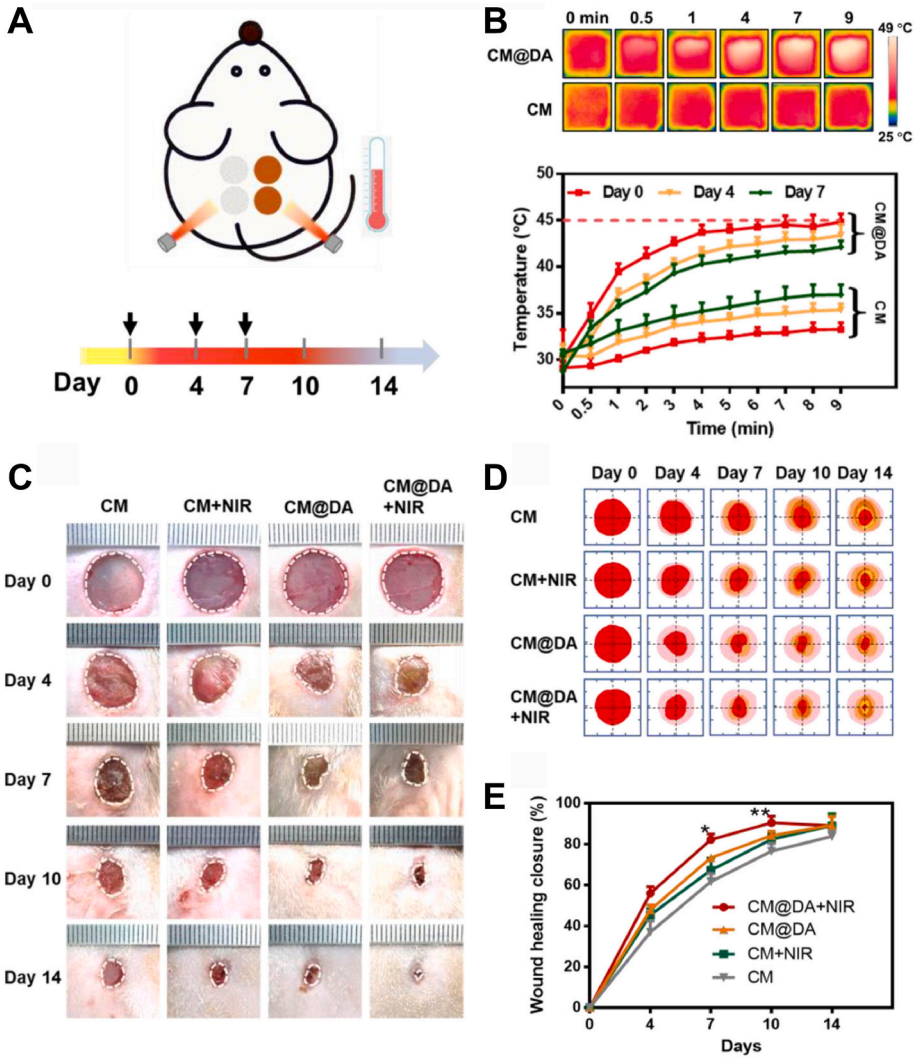

Fig. 3. A) Illustration of the *in vivo* treatment with an 808 nm NIR laser (0.7 W/cm^2) for 9 min. B) Representative *in vivo* infrared thermographic images (up) and temperature curves (bottom) of wounds under the NIR laser irradiation. C) Representative images of the wound treated groups at day 0, 4, 7, 10, and 14. D) Traces of wounds after different treatments (deep red area indicated the non-healing wounds). E) Analysis of wound healing closure versus treatment time. Reprinted from Applied Materials Today, Vol. 20, Y. Chen, M. Ye, L. Song, J. Zhang, Y. Yang, S. Luo, M. Lin, Q. Zhang, S. Li, Y. Zhou, A. Chen, Y. An, W. Huang, T. Xuan, Y. Gu, H. He, J. Wu, X. Li, Piezoelectric and photothermal dual functional film for enhanced dermal wound regeneration via upregulation of Hsp90 and HIF-1α, Pages No. 100756. Copyright (2020) with permission from Elsevier. (For interpretation of the references to colour in this figure legend, the reader is referred to the Web version of this article.)

Table 3
NIR-responsive biomaterials with a NIR light-triggered controlled release and application in the wound healing process. Note: The results refer to data obtained in *vivo* assays. (N.A.: Not Available).

Biomaterial	Composition	Therapeutic agent	Photo-triggered effect			Result	Ref
				Irradiation Parameters	Effect		
Hydrogel	BNN6-zeolitic imidazolate framework-8-PDA nanoparticles (1 mg/mL) encapsulated in a gelatin methacrylate/oxide dextran hydrogel (Gel/BZP)	NO released from BNN6	PTT	808 nm 2.0 W/cm^2 10 min	ΔT = 26.1 °C (*in vitro*)	The NIR-irradiated hydrogels released ≈ 7 μM of NO after 3 h, while the non-irradiated hydrogels only reached ≈ 4.8 μM. After the treatment with Gel/BZP + NIR, the wound area was 37.6 % and showed an enhanced vascularization and collagen deposition, while the wound area of Aquacel Ag, Gel/ZP + NIR, and Gel/BZP treated groups was 73.3 %, 47.5 %, and 43.3 %.	[33]
	Hydrogel based on dibenzaldehyde-grafted poly (ethylene glycol), lauric acid-CS, and curcumin-loaded mesoporous PDA nanoparticles (Gel-PDA@Cur)	Curcumin	PTT	808 nm 1.0 W/cm^2 10 min	ΔT = 24.8 °C	The NIR-irradiation promoted the release of ≈3.1 μg of Cur, while the non-irradiated group only reached ≈ 0.46 μg. After treatment with Gel-PDA@Cur + NIR, the were detected 89 CFU of *S. aureus*, while the 3 M, Cur, Gel, Gel + NIR, and Gel-PDA@Cur groups showed a lower efficacy with 3098, 2862, 3020, 2912, and 2812 CFU, respectively. After treatment with Gel-PDA@Cur + NIR, the wounds presented no bacteria infection, an enhanced collagen deposition, and reduced inflammatory response.	[41]
	*C*S-based hydrogel incorporated with mesoporous PDA nanoparticles-ciprofloxacin (2 mg/mL) and human epidermal growth factor (h-EGF-CS/β-GP-MPDA-Cip)	ciprofloxacin	PTT	808 nm N.A. 10 min	The temperature reached 47 °C (*in vitro*, 808 nm, 1.5 W/cm^2, 10 min)	The NIR-irradiation led to the release of ≈0.58 μg of ciprofloxacin, while the non-irradiated group only reached ≈ 0.27 μg. The h-EGF-CS/β-GP-MPDA@Cip + NIR group showed a decrease in the wound area to 9 % at day 8, while the blank, CS/β-GP-MPDA + NIR, CS/β-GP-MPDA@Cip, and CS/β-GP-MPDA@Cip + NIR groups showed a wound area of 39 %, 37 %, 23 %, and 15 %, respectively.	[80]
	Hydrogel based on poly (*N*-isopropylacrylamide) and methacrylated κ-carrageenan, incorporating polypyrrole-PDA nanoparticles and zeolitic imidazolate framework	Zn^{2+} released from zeolitic imidazolate framework-8	PTT	808 nm 2.5 W/cm^2 10 min	The temperature increased up to 50 °C	The NIR-irradiation led to a 2-times higher release of Zn^{2+}. After 14 days of treatment with MCA–NI–AA/NP/ZIF8+NIR, the wound closure reached the 91.8 %, with no living bacteria and a normal collagen deposition (densely packed and parallelly arranged collagen fibers).	[81]
Membrane	Polyvinylidene fluoride membrane loaded with UCNPs (10 %) and porphyrinic MOFs-l-arginine nanoparticles (UCNP@PCN@LA-PVDF)	NO released from l-arginine	PDT	N.A.	The DPBF absorbance with membrane + NIR decrease 20 %, while without NIR didn't change	The NIR-irradiation prompted the release of NO in the first 5 min reaching the maximum after 30 min After the treatment with UCNP@PCN@LA-PVDF + NIR, the *S. aureus* infected wounds presented no signs of bacteria, lower inflammatory cells, well-organized stratified epithelial layer, accelerated collagen deposition, and enhanced angiogenesis.	[46]
	Sodium nitroprusside doped PB nanoparticles (1 mg/mL) and Type I collagen incorporated into CS/poly (vinyl alcohol) nanofibers	NO released from Na_2 $[Fe(CN)_5NO]\cdot 2H_2O$ (SNP)	PTT	808 nm 1.0 W/cm^2	ΔT = ≈ 44 °C (*in vitro*, 808 nm, 0.5 W/cm^2, 6 min)	The NIR-irradiation led to a linear release of NO with the increase of irradiation time. After 10 days of treatment with the nanofibrous + NIR, the wound area was ≈0 %, showing a higher deposition of collagen fibers and no visible signs of infection. Control, NIR, and nanofibrous groups showed a reduction in the wound area of 16.6 %, 25.5 %, and 44.8 %, respectively.	[82]

(*continued on next page*)

Table 3 (*continued*)

Biomaterial	Composition	Therapeutic agent	Photo-triggered effect			Result	Ref
				Irradiation Parameters	Effect		
Nanostructure	Silica- carbon dots and bicarbonate nanoplataforms coated with PDA	CO_2 released from bicarbonate	PTT and PDT	5 min 808 nm 2.0 W/cm^2	ΔT = 30.1 °C TEMP/$^1O_2$ detected with NIR irradiation, while no signal was detectable without NIR	The NIR-irradiation led to a pronounced release of CO_2 from higher concentrations of nanomaterials (60, 120, and 240 mg/mL), while only residual amounts of CO_2 were released from lower concentrations (15 and 30 mg/mL). After 14 days of treatment with BC/QPCuRC@MSiO$_2$@PDA + NIR, the wound healing rate was 100 %, presenting the lowest number of bacterial colonies, no inflammatory cells, mature collagen fibers, and denser granulation tissue. Control + NIR, QPCuRC@MSiO$_2$ + NIR, and QPCuRC@MSiO$_2$@PDA + NIR groups showed a healing rate of 88 %, 92 %, and 94 %, respectively.	[83]
	Galactose- and fucose-based ligands on molybdenum disulfide	ceftazidime	PTT	5 min 808 nm 1.0 W/cm^2	ΔT = ≈ 30.9 °C	The ceftazidime was released in a NIR irradiation-dependent manner. After the treatment with Fuc-sheet@CAZ + NIR + white, the *P. aeruginosa*-infected wounds presented a wound size of ≈5 %, with the lower number of bacteria and increased collagen deposition. Control, ceftazidime and Fuc-sheet@CAZ, Fuc-sheet@CAZ + NIR, and Fuc-sheet@CAZ + white groups showed a wound size of ≈96 %, ≈91 %, ≈84 %, ≈63 %, and ≈33 %, respectively.	[84]
Microparticles	Microparticles comprised of silk fibroin, gelatin, agarose, and black phosphorus quantum dots (0.2 mg/mL) and loaded with fluorescein isothiocyanate-bovine serum albumin	Fluorescein isothiocyanate-bovine serum albumin	PTT	120 min 808 nm N.A.	ΔT = ≈15 °C/17 °C (*in vitro*, 808 nm, 2.41 W, 1.5 min)	The NIR-irradiation led to the release of 46 % of fluorescein isothiocyanate-bovine serum albumin, while non-irradiated group only reached 20 %. After treatment with the microparticles + NIR, the wound site presented enhanced angiogenesis, collagen deposition, granulation tissue formation, and no signs bacterial infection.	[85]

factor (h-EGF) to produce a NIR light-responsive drug delivery system aimed to enhance the wound healing process [80]. The MPDA@Cip nanoparticles showed a photothermal conversion efficiency of 32.3 % and could mediate an increase in the temperature to 52.9 °C under NIR laser irradiation (808 nm, 2 W/cm^2, 10 min). This heat generation leads to a porous gel and weakens the hydrogen bonding between Cip and MPDA, prompting the release of Cip, *i.e.*, triplicating the amount of Cip released after 3 h. Moreover, the treatment of *S. aureus*-infected full-thickness wounds showed that the NIR laser irradiation coupled with the faster Cip release enhanced the bactericidal activity of the hydrogel. Additionally, the wounds treated with h-EGF and Cip-loaded hydrogels plus NIR were completely healed in 10 days, showing a denser collagen matrix, increased tissue thickness, and a higher number of hair follicles [80].

3.2. Photodynamic therapy

The ROS generation in response to the NIR light can also be explored for accelerating wound healing, namely by treating bacterial infections or triggering the release of bioactive molecules. The efficacy of these treatments depends on several parameters such as the laser parameters, the photosensitizer, and oxygen availability (reviewed in detail in Refs. [54,87]).

3.2.1. Antibacterial properties

PDT has been showing high efficacy against different microorganisms such as bacteria, fungi, viruses, and parasites [25]. Nevertheless, their effect against bacteria has proven to be dependent on the bacterial strain [64,68]. The membrane of Gram-positive bacteria presents a more permeable structure, making them more susceptible to photosensitizers. In turn, the higher complexity of Gram-negative bacteria membrane, *i.e.*, additional outer membrane and lipopolysaccharides, has been associated with reduced uptake of external molecules [88,89]. Upon irradiation with the NIR laser, the generation of ROS can result in the direct oxidation of the bacterial cellular components (*e.g.*, cell membrane damage, DNA damage, and/or protein inactivation) and facilitate the transmembrane diffusion of intermediary reactive species, which ultimately lead to bacterial death [18,89]. Zhang et al. analyzed the effectiveness of polycaprolactone and polyvinylpyrrolidone-based nanofibers loaded with UCNPs containing hypericin for application in wound healing [61]. The authors observed that the fiber membranes reached the maximum ROS generation under NIR irradiation (808 nm, 0.5 W/cm^2, 20 min) at a concentration of 0.2 wt%. Of UCNPs-hypericin. The UCNPs-hypericin (0.20 wt%) plus NIR irradiation (808 nm, 20 min) reached a 97 % inhibition of Methicillin-resistant *S. aureus* bacteria, while the other groups did not elicit any significant bactericidal effect. In addition, the Methicillin-resistant *S. aureus* infected wounds treated with

the nanofibers incorporating UCNPs-hypericin, under NIR irradiation, exhibited a faster recovery rate compared with the other groups, presenting no bacteria colonies or any signs of infection after 3 days [61].

Apart from the single PDT treatment, researchers also have been exploring the combination with other therapeutics, such as PTT [42,63–65]. In fact, the increased temperature can enhance the membrane permeability which can lead to a higher effectiveness of the photosensitizers [90]. On the other hand, the presence of ROS can reduce bacterial resistance to heat which will contribute to the greater efficacy of hyperthermia [18,88]. In this regard, Du et al. produced 3-(trimethoxylmethosilyl) propyl methacrylate hydrogel incorporating Ag_2S quantum dots modified with mesoporous silica for the synergistic treatment of bacterial wound infections [47]. The hydrogels could mediate the temperature increase after NIR irradiation (808 nm, 1.8 W/cm^2, 4 min) to ≈ 46.1 °C, ≈60 °C, and 76.4 °C with the increase in the concentrations of Ag2S quantum dots (140 μg/mL, 280 μg/mL, and 420 μg/mL), respectively. Simultaneously, the ROS generation was confirmed by the resulting fluorescence signal of dichlorofluorescein diacetate. The combination of photothermal and photodynamic effects mediated by the hydrogels resulted in a 99.7 % and 99.8 % inhibition of *E. coli* and Methicillin-resistant *S. aureus,* respectively, upon NIR irradiation (808 nm, 1.8 W/cm^2, 4 min). Moreover, Methicillin-resistant *S. aureus* infected wounds treated with the hydrogel and NIR irradiation presented a faster wound healing process, with enhanced collagen deposition and angiogenesis at the infected sites, reduced number of colonies of bacteria, down-regulation of IL-6, and up-regulation of VEGF expression [47]. Similarly, Chu et al. produced quaternized Cu-carbon dots (Cu-RCDs-C35) as antibacterial platforms to mediate both photothermal and photodynamic effects in the treatment of bacterial infections [63]. The Cu-RCDs-C35 nanomaterials upon NIR irradiation (808 nm, 2 W/cm^2, 10 min) mediate a temperature increase up to 33.1–57.3 °C when the concentration ranged from 50 to 800 μg/mL. Additionally, the analysis of the fluorescence intensity of DCFH-DA in *E. coli* and *S. aureus*, after NIR irradiation (808 nm, 2 W/cm^2, 10 min), was indicative of the ROS generation. Such effect combinatorial effect led to an inhibition of 99.36 % and 99.98 % for *E. coli* and *S. aureus* treated with Cu-RCDs-C35 (800 μg/mL) plus NIR irradiation (808 nm, 2 W/cm^2, 10 min). Moreover, the treatment of *S. aureus*-infected wounds with Cu-RCDs-C35 plus NIR irradiation exhibited no signals of infection after 7 days and the healed area was superior to 95 % after 14 days with enhanced collagen deposition [63].

3.2.2. Drug delivery

The photodynamic effect can also be explored to mediate the drug release by exploring structural changes in the carrier [24,26]. The most common approaches are based on the hydrophobic to hydrophilic phase transitions or the cleavage of sensitive bonds (*e.g.*, poly (thioketal), selenium/tellurium containing polymers, and arylboronic acid/ester-containing polymers) [24]. Sun et al. developed a nitric oxide (NO)-assisted PDT mediated by a polyvinylidene fluoride membrane loaded with UCNPs and porphyrinic MOFs-L-arginine nanoparticles (UCNP@PCN@LA-PVDF) for the treatment of bacterial infections [46]. The ROS generation mediated by the UCNP@PCN@LA-PVDF membrane under NIR irradiation (980 nm, 0.5 W, 30 min) was confirmed by the 20 % decrease in the absorbance peak of 1,3-diphenylisobenzofuran (ROS indicator), while the non-irradiated groups maintained the initial absorbance during the study (Fig. 4D). Additionally, the ROS generation could also oxidize the L-arginine present in the membrane leading to the generation of NO, which contributed to the inhibition of 99.64 % and 99.63 % for *Pseudomonas aeruginosa* (*P. aeruginosa*) and *S. aureus*, respectively. In turn, the *S. aureus* infected wounds treated with UCNP@PCN@LA-PVDF and NIR irradiation showed a ≈95 % wound

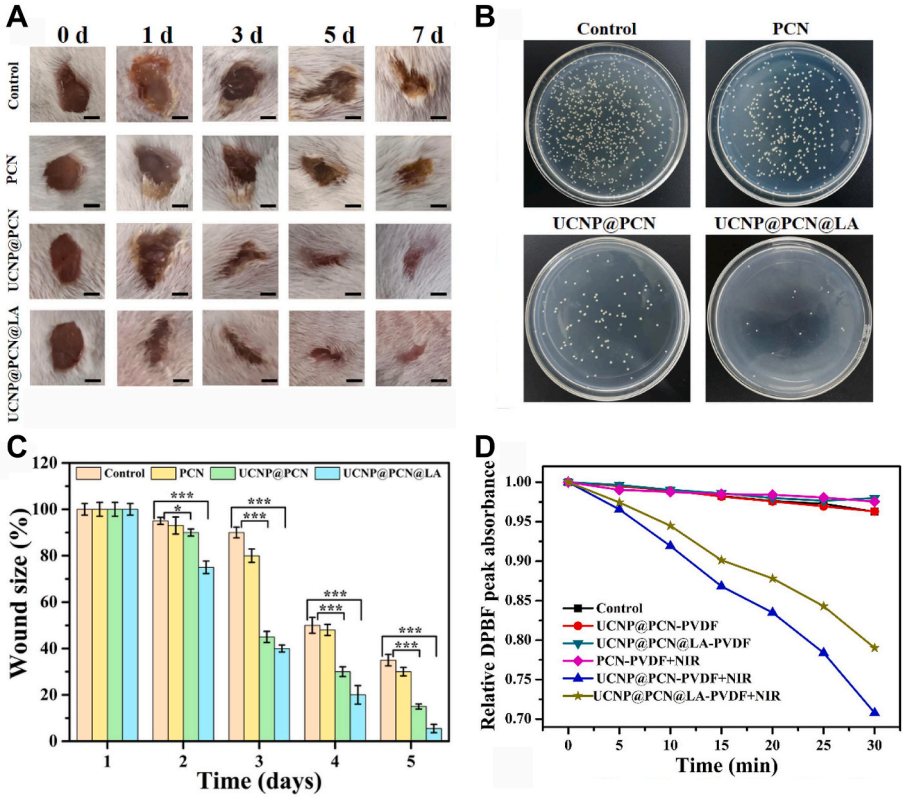

Fig. 4. A) Representative photographs of infected wounds after different treatments for 0, 1, 3, 5 and 7 days. B) Bacteria isolated from the mice's wounds on day 2. C) Evaluation of the relative wound area over time. D) Analysis of the absorption intensity of DPBF at 410 nm as a function of time with different samples. Reprinted from Chemical Engineering Journal, Vol. 417, J. Sun, Y. Fan, W. Ye, L. Tian, S. Niu, W. Ming, J. Zhao and L. Ren, Near-infrared light triggered photodynamic and nitric oxide synergistic antibacterial nanocomposite membrane, Pages No. 128049. Copyright (2021) with permission from Elsevier.

closure without any significative signs of infection (almost complete eradication of bacterial colonies), decreased presence of inflammatory cells, as well as a well-organized stratified epithelial layer, accelerated collagen deposition, and enhanced angiogenesis (Fig. 4) [46].

3.3. Photobiomodulation

PBMT is a non-invasive and non-heat-generating therapy in which different biological, chemical, and cellular processes are stimulated by exposition to light [91]. The light used in this therapy has low energy doses (*i.e.*, less than 10 J/cm^2) and a spectral range of 600–1070 nm. Different studies have shown that wavelengths in the NIR region and energy doses below 5 J/cm^2 are the most effective for regeneration purposes [92,93].

The PBMT effect is mediated by the light interaction with cellular photoacceptors, such as cytochrome C oxidase (CCO), cell membrane receptors (*e.g.*, Opsin 3 and 4), and even extracellular agents (*e.g.*, TGF-β1) [56,94]. For example, CCO can absorb NIR light, which results in the dissociation of the bounded NO. Furthermore, the CCO excitation by the NIR light also facilitates the electron transfer process, which increases ATP production and ROS generation [27,93,95]. Additionally, the PBMT can also activate ion channels leading to an increase of the Ca^{2+} levels and consequently the activation of several signaling pathways mediated by ROS, NO, cyclic adenosine monophosphate, and Ca^{2+} [93,94]. Moreover, in inflammatory situations, the NIR light can also stimulate the NF-kB production, reduce the expression of pro-inflammatory cytokines (TNF-α, IL-1β, IL-6, IL-8), and decrease the expression of matrix metalloproteinases [27,91,96]. So, in general, PBMT approaches accelerate the wound healing processes by controlling protein synthesis, extracellular matrix deposition, as well as cellular proliferation, differentiation, and migration [95,97–100]. Table 4 presents an overview of different studies demonstrating the effects of NIR photobiomodulation in the wound healing process.

In addition, this therapy also improves re-epithelialization and microcirculation, has anti-inflammatory effects, and reduces pain [95,109]. Keshri and collaborators studied the NIR laser application in the treatment of full-thickness third-degree burns [98]. The PBMT effect mediated by a pulsed NIR laser (810 nm, 10 Hz, average power 70 mW; average irradiance 40 mW/cm^2; total fluence 24 J/cm^2, duty cycle 50 %; pulse duration 50 msec; peak irradiance 80 mW/cm^2), 10 min exposure once daily for 7 days, led to a reduced inflammatory response (*i.e.*, lower levels of TNF-***α***, IL-1***β***, IL-6, and COX-2), increased collagen accumulation and stabilization (*i.e.*, 60 % and 56 % increase in hydroxyproline and hexosamine, respectively) as well as the cellular proliferation (*i.e.*, 30 % increase in DNA content) (please see Fig. 5). Moreover, the authors also observed advanced fibroblast proliferation, angiogenesis, and epidermal migration in the PBMT-treated wounds. These results translated in a faster wound contraction, a wound area of ≈40 % at day 8 contrasting with the ≈65 % in the control group, with no evidence of edema, bleeding, or wound exudates [98]. Similarly, Lau et al. analyzed the PBMT effects on the treatment of diabetic wounds [104]. The authors observed that the wound contraction was dependent on the power density of the NIR laser irradiation (808 nm, energy density 5 J/cm^2), wound contraction of 47.37 ± 31.17 %, 66.32 ± 22.53 %, 52.83 ± 27.98 % and 51.10 ± 26.89 % for the control group, 0.1 W/cm^2, 0.2 W/cm^2, and 0.3 W/cm^2 groups, respectively. Furthermore, at day 6, the group treated with a power density of 0.1 W/cm^2 showed an intense formation of granulation tissue, minimal to mild inflammatory cells at the dermis layer, and enhanced epithelization, whereas no significant improvements in the healing process were observed in the group treated with higher power density, 0.3 W/cm^2 [104].

3.4. Imaging

Apart from the enhancement of the healing process, it is also very important to be able to follow and monitor the progress of skin

Table 4
Overview of the NIR photobiomodulation effects on the wound healing process. Note: The results refer to data obtained in the *in vivo* assays. (N.A.: Not Available).

Spectrum	Duration	Power	Result	Ref
905 nm; 808 nm	10 s	1 kW ± 20 %, 5.19 J/cm^2	The NIR irradiation enabled the control of the fibroblast activation (induced by IL-1 and TNF-α) and the cessation of the persistent inflammation.	[96]
808 nm; 810 nm	10 min	40 mW/cm^2	The NIR irradiation enabled the attenuation of the inflammatory response including the decrease in TNF-α, IL-1β, IL-6, and COX-2 expression, enhanced cellular proliferation, collagen deposition, and extracellular matrix accumulation, as well as wound contraction.	[98]
808, 880; 1064 nm	50–250 s	20–100 mW/cm^2	The NIR irradiation with a wavelength of 808 nm and a power density of 40–60 mW/cm^2 resulted in the highest wound closure percentage (94.08 % ± 6.5 %).	[101]
808 nm	60 s	0.95 W/cm^2; 1 W/cm^2	The NIR irradiation enabled higher cell proliferation and migration, including a moderate increase in ROS production, stimulation of mitochondrial oxygen consumption, and ATP synthesis.	[100]
830, 980, and 2940 nm	110 s	0.5 W/cm^2	The NIR irradiation with a wavelength of 830 and 980 nm enabled a higher mitochondrial activity on fibroblasts, contrasting with the cellular apoptosis induced by the light with a wavelength of 2940 nm.	[102]
635, 730, 810, 980 nm	6.6 min	10 mW/cm^2	The NIR irradiation with a wavelength of 810 nm enhanced the wound healing, resulting in a significant reduction in the wound area, increased collagen accumulation, and complete re-epithelialization.	[103]
810 nm	10 min	40 mW/cm^2	The NIR irradiation prevented excessive inflammation and facilitated cellular proliferation, extracellular matrix accumulation, and tissue remodeling.	[97]
808 nm	17, 25, and 50 s	0.1, 0.2, and 0.3 W/cm^2	The NIR irradiation enabled the promotion of wound repair, including epithelialization and collagen fiber synthesis, showing the better results with a power density of 0.1 W/cm^2.	[104]
980 nm	25, 50, and 75 s	649.35 mW/cm^2	The NIR irradiation enabled the increase of the release of microvesicles from human keratinocytes.	[105]
450, 490, 550, 590, 650, 850 nm	N.A.	7–80 mW/cm^2	The NIR irradiation (850 nm) enabled the stimulation of human dermal fibroblasts, without intracellular ROS formation, while the blue	[106]

(*continued on next page*)

Table 4 (*continued*)

Spectrum	Duration	Power	Result	Ref
			light led to the inhibition of collagen production and human dermal fibroblasts' proliferation.	
632.8, 785, and 830 nm	1 min 58 s - 11 min 47 s	8.49 mW/cm^2	The NIR irradiation with a wavelength of 830 nm enabled an enhanced wound repair including migration of fibroblasts, deposition of collagen, and neovascularization.	[107]
980 nm	10, 25, 50, and 75 s	649.35 mW/cm^2	The NIR irradiation enabled an increase of NO production, which led to higher proliferation of keratinocytes and enhanced re-epithelialization.	[108]
830 nm	7 min 10 s	11.54 mW/cm^2	The NIR irradiation enabled cell viability, migration, and proliferation, which led to a better and more successful wound healing.	[27]

regeneration during the treatment (Table 5). NIR light can be explored to generate bioimages mainly through two different methodologies, fluorescence angiography and non-contact NIR imaging devices [28].

Fluorescence angiography is an invasive technique based on the intravenous injection of a fluorescent dye. After injection, images can be obtained upon excitation with NIR light and acquisition of the emitted fluorescence [28,50]. Du and co-workers developed gold nanostars modified with Methicillin-resistant *S. aureus*-identifiable aptamers and cypate nanoprobes (AuNS–Apt–Cy) via gelatinase-responsive linker for *in situ* NIR fluorescence imaging and localized PTT of *in vivo* Methicillin-resistant *S. aureus* infections [111]. The *in vitro* assays demonstrated that when in an enzymatic microenvironment of Methicillin-resistant *S. aureus* infection, the irradiation with NIR laser (808 nm, 0.5 W/cm^2, 5 min) resulted in the cypate fluorescence, whereas when incubated with *E. coli,* the cypate remains linked to the gold nanostars leading to the quenching of the fluorescence. Moreover, the application of AuNS–Apt–Cy in infected wounds of diabetic mice allowed the distinction between Methicillin-resistant *S. aureus* infected or *E. coli*-infected wounds using the NIR irradiation and further accelerated the wound healing process [111]. ICG is one most explored dyes in medicine, excitation peak at 789 nm and an emission peak at 814 nm, for assessing retinal blood vessels, liver function, and cardiac output [28,115]. Hoven et al. demonstrated that the intravenous administration of ICG could effectively allow the NIR fluorescence imaging of the amputation wound and further predict postoperative skin necrosis [50].

Non-contact NIR imaging devices allow a non-invasive, portable, and rapid wound monitoring. These images are based on the analysis of oxygenated or deoxygenated hemoglobin present in the tissues [28,116]. Hemoglobin presents different absorption spectra depending on the conjugation or not with oxygen, *i.e.*, deoxygenated hemoglobin presents an absorption peak at 750 nm, whereas oxygenated hemoglobin has an absorption peak at ≈ 850 nm [48,117]. Thus, it is possible to differentiate between injured and uninjured skin, since the uninjured skin has a lower degree of oxygenation when compared to the wound site [118]. For example, Lei et al. showed that a NIR optical scanner (NIROS) could differentiate healing from non-healing venous leg ulcers (VLU) based on differences in the blood flow that result in a positive and negative contrast, respectively [112]. Similarly, Kwasinski et al. also used NIROS to measure changes in oxy-, deoxy-, total hemoglobin, and oxygen saturation at the wound site [114]. The authors reported that the contrast from the wound to the surrounding tissue decreased and stabilized over time in healing wounds, whereas non-healing sites maintained the initial contrast value. Moreover, in slow-healing wounds, the authors observed that the contrast value varied but did not match that of the background tissue oxygenation [114].

In addition to that, NIR imaging can also be used as a theragnostic system for capturing wound physiological signals and triggering the treatment [119–122]. For example, Mei et al. developed Au/Ag core-shell nanorods for activatable NIR-II PTT and photoacoustic imaging of Methicillin-resistant *S. aureus* infection, monitoring the treatment progress [122]. The authors applied a matrigel with the nanorods and the activator (K_3 [$Fe(CN)_6$], to release the Ag^+) in Methicillin-resistant *S. aureus* infection sites in mice, and observed a 20-fold NIR-II photoacoustic signal increase. Furthermore, a maximum signal-to-background ratio of 9.5 was observed at 4 h post-injection, enabling the sensitive monitoring of Ag^+ release process. Moreover, the NIR-II PTT and release of free Ag^+ combinatorial treatment resulted in the almost complete healing of Methicillin-resistant *S. aureus*-infected wounds after 9 days, with no detection of residual live bacteria [122].

4. Adverse effects of NIR

Besides the advantages and different applications of NIR irradiation in the wound healing process, some concerns need to be considered for preventing undesirable side effects. Despite the high photothermal conversion efficiency of inorganic nanomaterials, these often present poor biodegradability. Therefore, they can accumulate in the human body and trigger some cytotoxic effects [38,123]. More importantly, the selection of the laser parameters, such as wavelength, intensity, and duration, will influence the light-tissue interaction [124,125]. In fact, different NIR light wavelengths present distinctive safety thresholds for human skin exposure. For example, the threshold safety for intensity in 808 nm light is around 0.33 W/cm^2, 0.54 W/cm^2 for 915 nm, and 0.72 W/cm^2 for 980 nm [124,126]. Moreover, some data indicates that the utilization of light with 808 nm or 915 nm wavelength can be safer than light with 980 nm since the absorption of water is higher at 980 nm [124]. Such was also demonstrated by Li et al. that observed an increase of 15.1 °C after irradiation with NIR laser (980 nm 1.0 W/cm^2), whereas when 808 nm or 915 nm light was used this value decreased to 3.0 °C and 3.4 °C, respectively [126]. This nonspecific tissue heating can trigger cell death and consequently tissue damage [124]. Furthermore, it is worth noting that patients with photosensitive conditions or those taking medication that increases sensitivity to light may experience adverse reactions to NIR light exposure [127]. In turn, eye exposure to high-intensity NIR light can also cause damage to the retina and affect the patient's eyesight [128,129]. Therefore, additional studies are still needed to further guarantee the safety of NIR-based therapies, since long-term effects of prolonged or repeated exposure are not fully understood and individual variability can lead to different reactions based on factors such as skin type, health conditions, and genetic variations.

5. Clinical trials

The application of NIR light-based therapies in wound regeneration, namely the PBMT effect and imaging capacity, and their translation potential have been evaluated in different clinical trials.

Several clinical trials already assessed the efficacy of the NIR laser treatment regimens in plastic and/or aesthetic surgery, focusing on the prevention of scar formation. For example, Capon et al. evaluated the ability of an 810 nm diode-laser system to accelerate the wound healing process of surgical scars [130]. For that purpose, 22 patients were treated with a high energy dose (80–130 J/cm^2) and 8 patients with a low energy dose (*i.e.*, inferior to 80 J/cm^2), NIR laser (810 nm and power up to 20 W), single irradiation after skin closure. After 12 months, the group treated with a high-energy dose reported an improvement rate in the quality and visual aspect of the scar of 60 % in the surgeon's analysis or 53.4 % in the patient's opinion. Moreover, these patients also described feeling less discomfort (*i.e.*, burning, itching, and prickling sensation) in the first 30 days after treatment. Nevertheless, the authors

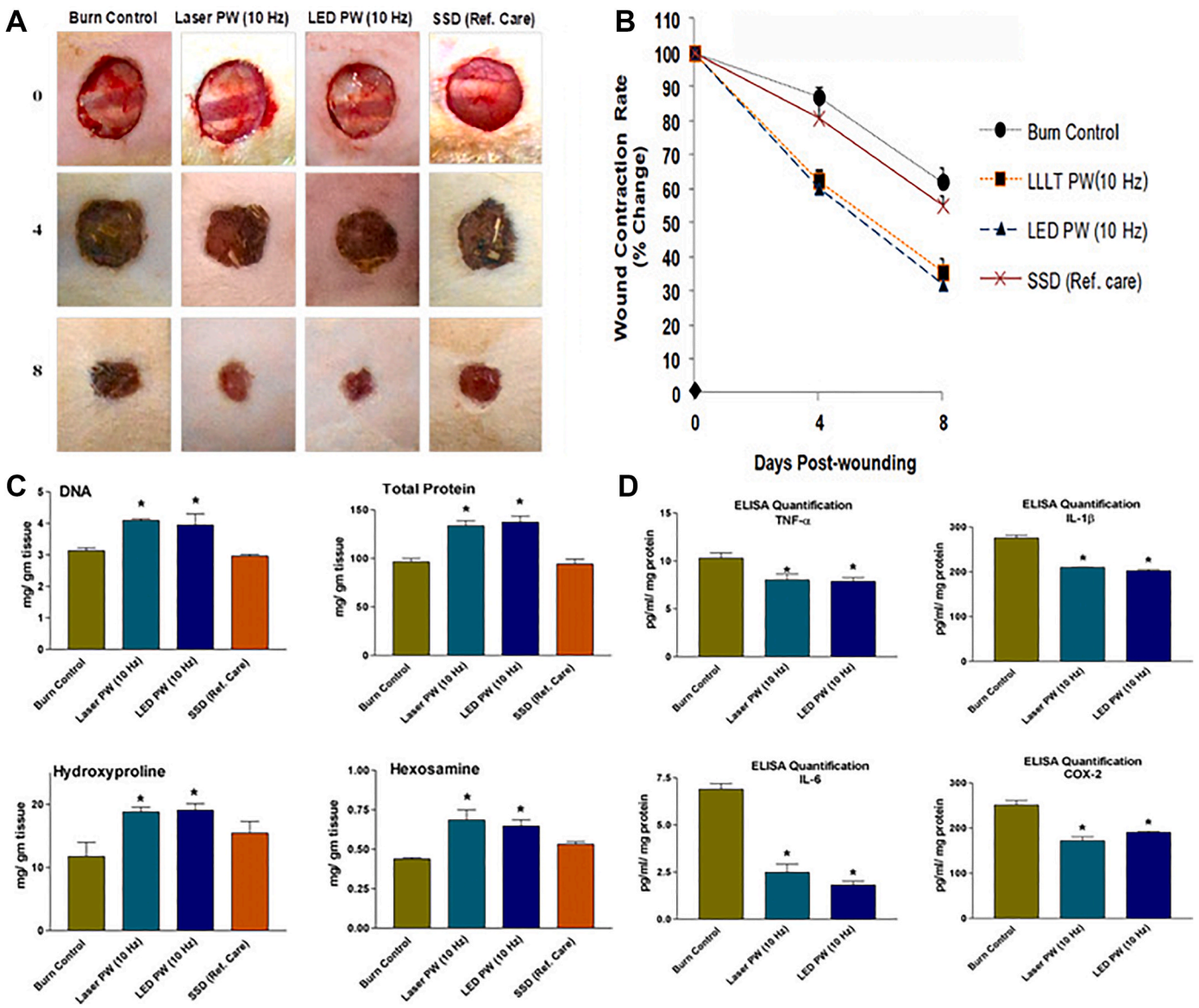

Fig. 5. A) Photomicrographs of the burn wounds treated with pulsed laser (810 nm), LED (808 ± 3 nm), or silver sulfadiazine. B) Analysis of the rate of wound area contraction. C) Effect of pulsed laser (810 nm), LED (808 ± 3 nm), or silver sulfadiazine on the pro-reparative markers. D) ELISA quantitative analyses of pro-inflammatory and pain markers in non-irradiated burn control, pulsed laser (810 nm), or LED (808 ± 3 nm) photobiomodulation treated burn wounds in rats. Reprinted from Journal of Photochemistry and Photobiology, Vol. 6, G. K. Keshri, G. Kumar, M. Sharma, K. Bora, B. Kumar and A. Gupta, Photobiomodulation effects of pulsed-NIR laser (810 nm) and LED (808 ± 3 nm) with identical treatment regimen on burn wound healing: A quantitative label-free global proteomic approach, Pages No. 100024. Copyright (2021) with permission from Elsevier.

also referred to the presence of superficial burns, without any negative long-term impact, in patients treated with higher energy doses, *i.e.*, 116, 127, and 127 J/cm^2. In turn, in the low-energy dose-treated patients no significant difference was detected between the irradiated and control region of the scar [130]. Similarly, Carvalho et al. investigated the effect of an infrared GaAlAs laser (830 nm) in the postsurgical scarring process [131]. The 28 patients were randomly divided into a control group and an experimental group, with irradiation, 40 mW, 13 J/cm^2, 24 h after surgery, and at days 3, 5, and 7. The obtained data showed improvements in the Vancouver Scar Scale analysis and the scar thickness measurements in the laser-treated group, preventing the formation of scar keloids and reducing the pain score by 50 % [131]. Haze and collaborators also evaluated a pulsed NIR 808 nm Ga-Al-As laser PBMT treatment regimen in diabetic foot ulcers [132]. Herein, the PBMT-treated group also presented a faster wound closure, *i.e.*, 70 % of the patients presented more than 90 % of wound closure, whereas this only occurred in 10 % of the control sham group. Otherwise, Longobardi et al. analyzed the measurement of hemoglobin O_2 saturation and the dimension of venous leg ulcers by NIR spectroscopy imaging [133]. The NIR spectroscopy 2D images acquired from 73 patients with venous leg ulcers enrolled in the study allowed not only to record the lesion dimensions but also the saturation levels of O_2. Moreover, the authors reported that the measurement of the O_2 saturation levels could be performed on the entire wound area or even in specific regions. Therefore, the NIR spectroscopy analysis of the venous leg ulcers allowed the clinicians to monitor and predict the wound healing progression in response to hyperbaric oxygen therapy [133].

6. Conclusions and future perspectives

Over the last few years, new wound dressings have been developed to further improve the wound healing process, however, they are still

Table 5
Overview of NIR-based imaging application in the wound healing process. Note: The results refer to data obtained in the *in vivo* assays. (N.A.: Not Available).

Biomaterial	Composition	Excitation/ emission wavelength	Results	Ref
Scaffold	collagen scaffold loaded with Ag_2S quantum dots-labeled human mesenchymal stem cells	808 nm/ NIR-II	The collagen scaffold loaded with Ag_2S quantum dots-labeled hMSCs enabled the visualization of the migration of transplanted hMSCs at the wound site for up to 1 month, through NIR-II fluorescence signals.	[51]
Nanostructure	fluorescent probe (AlkaP-1) based on benzoyl hydrazine-cy7 and a modified IR-780 molecule	720 nm/ 790 nm	The fluorescent probe (AlkaP-1) enabled the monitorization of the tissue alkalization (conversion of acute wounds to chronic wounds) through fluorescence changes.	[49]
	zeolitic imidazolate framework-8 - Ag_2S quantum dots, incorporating vancomycin	808 nm/ 1200 nm	The zeolitic imidazolate framework-8 - Ag_2S quantum dots, incorporating vancomycin enabled the *S. aureus* detection (limit of $\approx 1 \times 10^6$ CFU/ mL), through NIR-II fluorescence.	[110]
	nanoprobe based on gold nanostars functionalized with Methicillin-resistant *S. aureus*-identifiable aptamer and gelatinase-responsive heptapeptide linker–cypate complexes (AuNS–Apt–Cy)	808 nm/ 850 nm	The AuNS–Apt–Cy nanoprobe enabled the NIR fluorescence imaging with high sensitivity (10^5 CFU), and mediated PTT in Methicillin-resistant *S. aureus* infections.	[111]
N.A.	N.A.	830 nm	The NIR imaging enabled the differentiation of healing from non-healing regions in wounds, using a noncontact wide-area imager.	[112]
		710 nm, 830 nm/> 645 nm	The NIR imaging enabled the differentiation of healing from non-healing regions in diabetic foot lesions, through optical contrast between wound and adjacent tissue.	[113]
		725, 797 nm	The NIR imaging enabled the differentiation of healing from non-healing regions through the measurement of changes in oxy-, deoxy-, total hemoglobin, and oxygen saturation.	[114]

associated with some limitations such as uncontrolled drug delivery and limited therapeutic effectiveness. In this field, biomaterials responsive to NIR light have been investigated as a low-invasive technique to trigger localized treatments with minimal damage to the surrounding tissues. These therapeutic approaches are based on photothermal and/or photodynamic effects that lead to heat and ROS generation, respectively. Heat generation can cause different effects depending on the maximum temperature that is achieved, *i.e.*, small temperature increases can promote cell proliferation and angiogenesis, while high temperatures can effectively improve the antibacterial properties of the materials. Furthermore, this effect can also be explored to control the release of different therapeutic molecules and improve the wound healing process. In the same way, ROS generation can also be explored to treat bacterial infections or trigger the release of bioactive molecules. In addition, the NIR light is also used as a non-heat-generating therapy, namely in PBMT, in which different biological, chemical, and cellular processes are stimulated by the exposition to the light. Apart from these effects, the NIR light can also enable the monitorization of the wound healing process through bioimaging approaches.

In conclusion, the NIR light holds high potential for improving the wound healing process through different approaches. More importantly, this approach overcomes the issue of multi-drug resistance, since it imprints an antibacterial effect without resorting to the use of antibiotics. Furthermore, it enables a controlled treatment both in time and space, which also improves the wound healing process.

Despite the clinical trials already covering the fields of PBMT and bioimaging, there are still several studies that need to be considered before considering the translation to the clinic of NIR-responsive biomaterials aimed for the treatment of infected wounds. In fact, in this area, nowadays the clinical applications of NIR light are limited to the reduction of inflammation and pain both in muscles and joints, as well as in the improvement of the skin's visual appearance. Moreover, biocompatible photosensitive materials and singlet oxygen-sensitive linkers still require higher exploration to improve the light conversion efficiency as well as the development of photocontrolled drug delivery systems. Additionally, the validation of new materials and the capacity to scale up the production methods are also important topics for achieving the successful translation of NIR-based wound healing therapeutics.

CRediT authorship contribution statement

Mariana F.P. Graça: Conceptualization, Writing – original draft. **André F. Moreira:** Conceptualization, Supervision, Writing – review & editing. **Ilídio J. Correia:** Funding acquisition, Supervision, Writing – review & editing.

Declaration of competing interest

The authors declare the following financial interests/personal relationships which may be considered as potential competing interests: Ilidio J. Correia reports financial support was provided by Foundation for Science and Technology. Andre F. Moreira reports financial support was provided by Foundation for Science and Technology. Mariana F. P. Graca reports financial support was provided by Foundation for Science and Technology. Andre F. Moreira reports financial support was provided by Fundo Europeu de Desenvolvimento Regional. Ilidio J. Correia reports financial support was provided by Fundo Europeu de Desenvolvimento Regional.

Data availability

No data was used for the research described in the article.

Acknowledgments

This work was developed within the scope of the CICS-UBI projects UIDB/00709/2020 and UIDP/00709/2020, financed by national funds through the Portuguese Foundation for Science and Technology/MCTES. The funding from 2022.06320.PTDC and PTDC/BTABTA/0696/2020 are also acknowledged. Mariana F. P. Graça acknowledge funding from individual Ph.D. fellowships from FCT (2021.08657.BD).

References

[1] A. Guerra, J. Belinha, R.N. Jorge, Modelling skin wound healing angiogenesis: a review, J. Theor. Biol. 459 (2018) 1–17, https://doi.org/10.1016/j.jtbi.2018.09.020.
[2] E. Rezvani Ghomi, S. Khalili, S. Nouri Khorasani, R. Esmaeely Neisiany, S. Ramakrishna, Wound dressings: current advances and future directions, J. Appl. Polym. Sci. 136 (27) (2019) 47738, https://doi.org/10.1002/app.47738.
[3] Q. Zeng, X. Qi, G. Shi, M. Zhang, H. Haick, Wound dressing: from nanomaterials to diagnostic dressings and healing evaluations, ACS Nano 16 (2) (2022) 1708–1733, https://doi.org/10.1021/acsnano.1c08411.
[4] R.S. Sequeira, S.P. Miguel, C.S. Cabral, A.F. Moreira, P. Ferreira, I.J. Correia, Development of a poly (vinyl alcohol)/lysine electrospun membrane-based drug delivery system for improved skin regeneration, Int. J. Pharm. 570 (2019) 118640, https://doi.org/10.1016/j.ijpharm.2019.118640.
[5] S.P. Miguel, D.R. Figueira, D. Simões, M.P. Ribeiro, P. Coutinho, P. Ferreira, I. J. Correia, Electrospun polymeric nanofibres as wound dressings: a review, Colloids Surf., B 169 (2018) 60–71, https://doi.org/10.1016/j.colsurfb.2018.05.011.
[6] M. Mirhaj, M. Tavakoli, J. Varshosaz, S. Labbaf, F. Jafarpour, P. Ahmaditabar, S. Salehi, N. Kazemi, Platelet rich fibrin containing nanofibrous dressing for wound healing application: fabrication, characterization and biological evaluations, Biomater. Adv. 134 (2022) 112541, https://doi.org/10.1016/j.msec.2021.112541.
[7] H. Zhang, X. Sun, J. Wang, Y. Zhang, M. Dong, T. Bu, L. Li, Y. Liu, L. Wang, Multifunctional injectable hydrogel dressings for effectively accelerating wound healing: enhancing biomineralization strategy, Adv. Funct. Mater. 31 (23) (2021) 2100093, https://doi.org/10.1002/adfm.202100093.
[8] Z. Liang, P. Lai, J. Zhang, Q. Lai, L. He, Impact of moist wound dressing on wound healing time: a meta-analysis, Int. Wound J. (2023) 1–12, https://doi.org/10.1111/iwj.14319.
[9] B. Cullen, A. Gefen, The biological and physiological impact of the performance of wound dressings, Int. Wound J. 20 (4) (2023) 1292–1303, https://doi.org/10.1111/iwj.13960.
[10] C. Huang, W. Yuan, J. Chen, L.-P. Wu, T. You, Construction of smart biomaterials for promoting diabetic wound healing, Molecules 28 (3) (2023) 1110, https://doi.org/10.3390/molecules28031110.
[11] S. Ren, S. Guo, L. Yang, C. Wang, Effect of composite biodegradable biomaterials on wound healing in diabetes, Front. Bioeng. Biotechnol. 10 (2022) 1060026, https://doi.org/10.3389/fbioe.2022.1060026.
[12] S. Dhivya, V.V. Padma, E. Santhini, Wound dressings–a review, Biomedicine 5 (4) (2015) 22, https://doi.org/10.7603/s40681-015-0022-9.
[13] E. Cheah, Z. Wu, S.S. Thakur, S.J. O'Carroll, D. Svirskis, Externally triggered release of growth factors-A tissue regeneration approach, J. Contr. Release 332 (2021) 74–95, https://doi.org/10.1016/j.jconrel.2021.02.015.
[14] H. Samadian, H. Maleki, Z. Allahyari, M. Jaymand, Natural polymers-based light-induced hydrogels: promising biomaterials for biomedical applications, Coord. Chem. Rev. 420 (2020) 213432, https://doi.org/10.1016/j.ccr.2020.213432.
[15] M.A.M. Jahromi, P.S. Zangabad, S.M.M. Basri, K.S. Zangabad, A. Ghamarypour, A.R. Aref, M. Karimi, M.R. Hamblin, Nanomedicine and advanced technologies for burns: preventing infection and facilitating wound healing, Adv. Drug Deliv. Rev. 123 (2018) 33–64, https://doi.org/10.1016/j.addr.2017.08.001.
[16] L. Lin, X. Song, X. Dong, B. Li, Nano-photosensitizers for enhanced photodynamic therapy, Photodiagnosis Photodyn. Ther. 36 (2021) 102597, https://doi.org/10.1016/j.pdpdt.2021.102597.
[17] K. Shanmugapriya, H.W. Kang, Engineering pharmaceutical nanocarriers for photodynamic therapy on wound healing: review, Mater. Sci. Eng. C 105 (2019) 110110, https://doi.org/10.1016/j.msec.2019.110110.
[18] Y. Chen, Y. Gao, Y. Chen, L. Liu, A. Mo, Q. Peng, Nanomaterials-based photothermal therapy and its potentials in antibacterial treatment, J. Contr. Release 328 (2020) 251–262, https://doi.org/10.1016/j.jconrel.2020.08.055.
[19] G. Cheng, B. Li, Nanoparticle-based photodynamic therapy: new trends in wound healing applications, Mater. Today Adv. 6 (2020) 100049, https://doi.org/10.1016/j.mtadv.2019.100049.
[20] L. Sheng, Z. Zhang, Y. Zhang, E. Wang, B. Ma, Q. Xu, L. Ma, M. Zhang, G. Pei, J. Chang, A novel "hot spring"-mimetic hydrogel with excellent angiogenic properties for chronic wound healing, Biomaterials 264 (2021) 120414, https://doi.org/10.1016/j.biomaterials.2020.120414.
[21] X. Zhang, B. Tan, Y. Wu, M. Zhang, X. Xie, J. Liao, An injectable, self-healing carboxymethylated chitosan hydrogel with mild photothermal stimulation for wound healing, Carbohydr. Polym. 293 (2022) 119722, https://doi.org/10.1016/j.carbpol.2022.119722.
[22] Y. Chu, S. Chai, F. Li, C. Han, X. Sui, T. Liu, Combined strategy of wound healing using thermo-sensitive PNIPAAm hydrogel and CS/PVA membranes: development and in-vivo evaluation, Polymers 14 (12) (2022) 2454, https://doi.org/10.3390/polym14122454.
[23] X. Zhang, B. Tan, Y. Wu, M. Zhang, J. Liao, A review on hydrogels with photothermal effect in wound healing and bone tissue engineering, Polymers 13 (13) (2021) 2100, https://doi.org/10.3390/polym13132100.
[24] C.G. Dariva, J.F. Coelho, A.C. Serra, Near infrared light-triggered nanoparticles using singlet oxygen photocleavage for drug delivery systems, J. Contr. Release 294 (2019) 337–354, https://doi.org/10.1016/j.jconrel.2018.12.042.
[25] X. Hu, H. Zhang, Y. Wang, B.-C. Shiu, J.-H. Lin, S. Zhang, C.-W. Lou, T.-T. Li, Synergistic antibacterial strategy based on photodynamic therapy: progress and perspectives, Chem. Eng. J. 450 (2022) 138129, https://doi.org/10.1016/j.cej.2022.138129.
[26] Y. Tang, G. Wang, NIR light-responsive nanocarriers for controlled release, J. Photochem. Photobiol., C 47 (2021) 100420, https://doi.org/10.1016/j.jphotochemrev.2021.100420.
[27] O. Oyebode, N.N. Houreld, H. Abrahamse, Photobiomodulation in diabetic wound healing: a review of red and near-infrared wavelength applications, Cell Biochem. Funct. 39 (5) (2021) 596–612, https://doi.org/10.1002/cbf.3629.
[28] J. Arnold, V.L. Marmolejo, Interpretation of near-infrared imaging in acute and chronic wound care, Diagnostics 11 (5) (2021) 778, https://doi.org/10.3390/diagnostics11050778.
[29] Y. Yang, J. Aw, B. Xing, Nanostructures for NIR light-controlled therapies, Nanoscale 9 (11) (2017) 3698–3718, https://doi.org/10.1039/C6NR09177F.
[30] H.U. Kim, T. Kim, C. Kim, M. Kim, T. Park, Recent advances in structural design of efficient near-infrared light-emitting organic small molecules, Adv. Funct. Mater. 33 (1) (2023) 2208082, https://doi.org/10.1002/adfm.202208082.
[31] W. Zhao, Y. Zhao, Q. Wang, T. Liu, J. Sun, R. Zhang, Remote light-responsive nanocarriers for controlled drug delivery: advances and perspectives, Small 15 (45) (2019) 1903060, https://doi.org/10.1002/smll.201903060.
[32] S. Golovynskyi, I. Golovynska, L.I. Stepanova, O.I. Datsenko, L. Liu, J. Qu, T. Y. Ohulchanskyy, Optical windows for head tissues in near-infrared and short-wave infrared regions: approaching transcranial light applications, J. Biophot. 11 (12) (2018) e201800141, https://doi.org/10.1002/jbio.201800141.
[33] H. Liu, X. Zhu, H. Guo, H. Huang, S. Huang, S. Huang, W. Xue, P. Zhu, R. Guo, Nitric oxide released injectable hydrogel combined with synergistic photothermal therapy for antibacterial and accelerated wound healing, Appl. Mater. Today 20 (2020) 100781, https://doi.org/10.1016/j.apmt.2020.100781.
[34] L. Han, P. Li, P. Tang, X. Wang, T. Zhou, K. Wang, F. Ren, T. Guo, X. Lu, Mussel-inspired cryogels for promoting wound regeneration through photobiostimulation, modulating inflammatory responses and suppressing bacterial invasion, Nanoscale 11 (34) (2019) 15846–15861, https://doi.org/10.1039/C9NR03095F.
[35] S.Y. Tee, K.Y. Win, S.S. Goh, C.P. Teng, K.Y. Tang, M.D. Regulacio, Z. Li, E. Ye, Introduction to photothermal nanomaterials, in: E. Ye, Z. Li (Eds.), Photothermal Nanomaterials, RSC Polym. Chem. Ser.: Croydon., 2022, pp. 1–32.
[36] Y. Shi, M. Liu, F. Deng, G. Zeng, Q. Wan, X. Zhang, Y. Wei, Recent progress and development on polymeric nanomaterials for photothermal therapy: a brief overview, J. Mater. Chem. B 5 (2) (2017) 194–206, https://doi.org/10.1039/C6TB02249A.
[37] J. Li, W. Zhang, W. Ji, J. Wang, N. Wang, W. Wu, Q. Wu, X. Hou, W. Hu, L. Li, Near infrared photothermal conversion materials: mechanism, preparation, and photothermal cancer therapy applications, J. Mater. Chem. B 9 (38) (2021) 7909–7926, https://doi.org/10.1039/D1TB01310F.
[38] Y. Wang, H.-M. Meng, Z. Li, Near-infrared inorganic nanomaterial-based nanosystems for photothermal therapy, Nanoscale 13 (19) (2021) 8751–8772, https://doi.org/10.1039/D1NR00323B.
[39] Z. Bao, X. Liu, Y. Liu, H. Liu, K. Zhao, Near-infrared light-responsive inorganic nanomaterials for photothermal therapy, Asian J. Pharm. Sci. 11 (3) (2016) 349–364, https://doi.org/10.1016/j.ajps.2015.11.123.
[40] Y. Zhang, Y. Liu, Z. Guo, F. Li, H. Zhang, F. Bai, L. Wang, Chitosan-based bifunctional composite aerogel combining absorption and phototherapy for

bacteria elimination, Carbohydr. Polym. 247 (2020) 116739, https://doi.org/10.1016/j.carbpol.2020.116739.
[41] B. Tao, C. Lin, Z. Yuan, Y. He, M. Chen, K. Li, J. Hu, Y. Yang, Z. Xia, K. Cai, Near infrared light-triggered on-demand Cur release from Gel-PDA@Cur composite hydrogel for antibacterial wound healing, Chem. Eng. J. 403 (2021) 126182, https://doi.org/10.1016/j.cej.2020.126182.
[42] X. Zhou, Z. Wang, Y.K. Chan, Y. Yang, Z. Jiao, L. Li, J. Li, K. Liang, Y. Deng, Infection micromilieu-activated nanocatalytic membrane for orchestrating rapid sterilization and stalled chronic wound regeneration, Adv. Funct. Mater. 32 (7) (2022) 2109469, https://doi.org/10.1002/adfm.202109469.
[43] Z. Cao, D. Li, J. Wang, X. Yang, Reactive oxygen species-sensitive polymeric nanocarriers for synergistic cancer therapy, Acta Biomater. 130 (2021) 17–31, https://doi.org/10.1016/j.actbio.2021.05.023.
[44] M.K. Mahata, R. De, K.T. Lee, Near-infrared-triggered upconverting nanoparticles for biomedicine applications, Biomedicines 9 (7) (2021) 756, https://doi.org/10.3390/biomedicines9070756.
[45] L. Beauté, N. McClenaghan, S. Lecommandoux, Photo-triggered polymer nanomedicines: from molecular mechanisms to therapeutic applications, Adv. Drug Deliv. Rev. 138 (2019) 148–166, https://doi.org/10.1016/j.addr.2018.12.010.
[46] J. Sun, Y. Fan, W. Ye, L. Tian, S. Niu, W. Ming, J. Zhao, L. Ren, Near-infrared light triggered photodynamic and nitric oxide synergistic antibacterial nanocomposite membrane, Chem. Eng. J. 417 (2021) 128049, https://doi.org/10.1016/j.cej.2020.128049.
[47] T. Du, Z. Xiao, J. Cao, L. Wei, C. Li, J. Jiao, Z. Song, J. Liu, X. Du, S. Wang, NIR-activated multi-hit therapeutic Ag2S quantum dot-based hydrogel for healing of bacteria-infected wounds, Acta Biomater. 145 (2022) 88–105, https://doi.org/10.1016/j.actbio.2022.04.013.
[48] A.S. Landsman, D. Barnhart, M. Sowa, Near-infrared spectroscopy imaging for assessing skin and wound oxygen perfusion, Clin. Podiatr. Med. Surg. 35 (3) (2018) 343–355, https://doi.org/10.1016/j.cpm.2018.02.005.
[49] H. Mai, Y. Wang, S. Li, R. Jia, S. Li, Q. Peng, Y. Xie, X. Hu, S. Wu, A pH-sensitive near-infrared fluorescent probe with alkaline p K a for chronic wound monitoring in diabetic mice, Chem. Commun. 55 (51) (2019) 7374–7377, https://doi.org/10.1039/C9CC02289A.
[50] P. Van Den Hoven, S.D. Van Den Berg, J.P. Van Der Valk, H. Van Der Krogt, L. P. Van Doorn, K.E.A. Van De Bogt, J. Van Schaik, A. Schepers, A.L. Vahrmeijer, J. F. Hamming, J.R. Van Der Vorst, Assessment of tissue viability following amputation surgery using near-infrared fluorescence imaging with indocyanine green, Ann. Vasc. Surg. 78 (2022) 281–287, https://doi.org/10.1016/j.avsg.2021.04.030.
[51] G. Chen, F. Tian, C. Li, Y. Zhang, Z. Weng, Y. Zhang, R. Peng, Q. Wang, In vivo real-time visualization of mesenchymal stem cells tropism for cutaneous regeneration using NIR-II fluorescence imaging, Biomaterials 53 (2015) 265–273, https://doi.org/10.1016/j.biomaterials.2015.02.090.
[52] P. Chinna Ayya Swamy, G. Sivaraman, R.N. Priyanka, S.O. Raja, K. Ponnuvel, J. Shanmugpriya, A. Gulyani, Near Infrared (NIR) absorbing dyes as promising photosensitizer for photo dynamic therapy, Coord. Chem. Rev. 411 (2020) 213233, https://doi.org/10.1016/j.ccr.2020.213233.
[53] A. Sahu, J.H. Lee, H.G. Lee, Y.Y. Jeong, G. Tae, Prussian blue/serum albumin/indocyanine green as a multifunctional nanotheranostic agent for bimodal imaging guided laser mediated combinatorial photothera py, J. Contr. Release 236 (2016) 90–99, https://doi.org/10.1016/j.jconrel.2016.06.031.
[54] D. de Melo-Diogo, C. Pais-Silva, D.R. Dias, A.F. Moreira, I.J. Correia, Strategies to improve cancer photothermal therapy mediated by nanomaterials, Adv. Healthcare Mater. 6 (10) (2017) 1700073, https://doi.org/10.1002/adhm.201700073.
[55] N. Fernandes, C.F. Rodrigues, A.F. Moreira, I.J. Correia, Overview of the application of inorganic nanomaterials in cancer photothermal therapy, Biomater. Sci. 8 (11) (2020) 2990–3020, https://doi.org/10.1039/D0BM00222D.
[56] Z. Chen, S. Huang, M. Liu, The review of the light parameters and mechanisms of Photobiomodulation on melanoma cells, Photodermatol. Photoimmunol. Photomed. 38 (1) (2022) 3–11, https://doi.org/10.1111/phpp.12715.
[57] V. Vivcharenko, M. Trzaskowska, A. Przekora, Wound dressing modifications for accelerated healing of infected wounds, Int. J. Mol. Sci. 24 (8) (2023) 7193, https://doi.org/10.3390/ijms24087193.
[58] K. Zegadło, M. Gieroń, P. Żarnowiec, K. Durlik-Popińska, B. Kręcisz, W. Kaca, G. Czerwonka, Bacterial motility and its role in skin and wound infections, Int. J. Mol. Sci. 24 (2) (2023) 1707, https://doi.org/10.3390/ijms24021707.
[59] Z. Ahmadian, H. Gheybi, M. Adeli, Efficient wound healing by antibacterial property: advances and trends of hydrogels, hydrogel-metal NP composites and photothermal therapy platforms, J. Drug Deliv. Sci. Technol. 73 (2022) 103458, https://doi.org/10.1016/j.jddst.2022.103458.
[60] S. Arbab, H. Ullah, M.I.U. Khan, M.N.K. Khattak, J. Zhang, K. Li, I.U. Hassan, Diversity and distribution of thermophilic microorganisms and their applications in biotechnology, J. Basic Microbiol. 62 (2) (2022) 95–108, https://doi.org/10.1002/jobm.202100529.
[61] J. Zhang, C.-L. Liu, J.-J. Liu, X.-H. Bai, Z.-K. Cao, J. Yang, M. Yu, S. Ramakrishna, Y.-Z. Long, Eluting mode of photodynamic nanofibers without photosensitizer leakage for one-stop treatment of outdoor hemostasis and sterilizing superbacteria, Nanoscale 13 (12) (2021) 6105–6116, https://doi.org/10.1039/D1NR00179E.
[62] L. Chen, D. Zhang, K. Cheng, W. Li, Q. Yu, L. Wang, Photothermal-responsive fiber dressing with enhanced antibacterial activity and cell manipulation towards promoting wound-healing, J. Colloid Interface Sci. 623 (2022) 21–33, https://doi.org/10.1016/j.jcis.2022.05.013.
[63] X. Chu, P. Zhang, Y. Wang, B. Sun, Y. Liu, Q. Zhang, W. Feng, Z. Li, K. Li, N. Zhou, Near-infrared carbon dot-based platform for bioimaging and photothermal/photodynamic/quaternary ammonium triple synergistic sterilization triggered by single NIR light source, Carbon 176 (2021) 126–138, https://doi.org/10.1016/j.carbon.2021.01.119.
[64] B. Tao, C. Lin, A. Guo, Y. Yu, X. Qin, K. Li, H. Tian, W. Yi, D. Lei, L. Chen, Fabrication of copper ions-substituted hydroxyapatite/polydopamine nanocomposites with high antibacterial and angiogenesis effects for promoting infected wound healing, J. Ind. Eng. Chem. 104 (2021) 345–355, https://doi.org/10.1016/j.jiec.2021.08.035.
[65] Y. Fan, Z. Wang, W. Ren, G. Liu, J. Xing, T. Xiao, W. Li, Y. Li, P. Yu, C. Ning, Space-confined synthesis of thin polypyrrole nanosheets in layered bismuth oxychloride for a photoresponse antibacterial within the near-infrared window and accelerated wound healing, ACS Appl. Mater. Interfaces 14 (32) (2022) 36966–36979, https://doi.org/10.1021/acsami.2c11503.
[66] C. Tong, X. Zhong, Y. Yang, X. Liu, G. Zhong, C. Xiao, B. Liu, W. Wang, X. Yang, PB@ PDA@ Ag nanosystem for synergistically eradicating MRSA and accelerating diabetic wound healing assisted with laser irradiation, Biomaterials 243 (2020) 119936, https://doi.org/10.1016/j.biomaterials.2020.119936.
[67] X. Qi, W. Pan, X. Tong, T. Gao, Y. Xiang, S. You, R. Mao, J. Chi, R. Hu, W. Zhang, ε-Polylysine-stabilized agarose/polydopamine hydrogel dressings with robust photothermal property for wound healing, Carbohydr. Polym. 264 (2021) 118046, https://doi.org/10.1016/j.carbpol.2021.118046.
[68] X. Wang, X. Sun, T. Bu, K. Xu, L. Li, M. Li, R. Li, L. Wang, Germanene-modified chitosan hydrogel for treating bacterial wound infection: an ingenious hydrogel-assisted photothermal therapy strategy, Int. J. Biol. Macromol. 221 (2022) 1558–1571, https://doi.org/10.1016/j.ijbiomac.2022.09.128.
[69] Y. Luo, X. Zhou, C. Liu, R. Lu, M. Jia, P. Li, S. Zhang, Scavenging ROS and inflammation produced during treatment to enhance the wound repair efficacy of photothermal injectable hydrogel, Biomater. Adv. 141 (2022) 213096, https://doi.org/10.1016/j.bioadv.2022.213096.
[70] X. Lei, M. Li, C. Wang, P. Cui, L. Qiu, S. Zhou, P. Jiang, H. Li, D. Zhao, X. Ni, J. Wang, J. Xia, Degradable microneedle patches loaded with antibacterial gelatin nanoparticles to treat staphylococcal infection-induced chronic wounds, Int. J. Biol. Macromol. 217 (2022) 55–65, https://doi.org/10.1016/j.ijbiomac.2022.07.021.
[71] X. Yi, Q.-Y. Duan, F.-G. Wu, Low-temperature photothermal therapy: strategies and applications, Res. 2021 (2021) 1–38, https://doi.org/10.34133/2021/9816594.
[72] Y. Chen, M. Ye, L. Song, J. Zhang, Y. Yang, S. Luo, M. Lin, Q. Zhang, S. Li, Y. Zhou, A. Chen, Y. An, W. Huang, T. Xuan, Y. Gu, H. He, J. Wu, X. Li, Piezoelectric and photothermal dual functional film for enhanced dermal wound regeneration via upregulation of Hsp90 and HIF-1α, Appl. Mater. Today 20 (2020) 100756 https://doi.org/10.1016/j.apmt.2020.100756.
[73] M.W. Hance, K.D. Nolan, J.S. Isaacs, The double-edged sword: conserved functions of extracellular hsp90 in wound healing and cancer, Cancers 6 (2) (2014) 1065–1097, https://doi.org/10.3390/cancers6021065.
[74] X. Dong, J. Ye, Y. Chen, T. Tanziela, H. Jiang, X. Wang, Intelligent peptide-nanorods against drug-resistant bacterial infection and promote wound healing by mild-temperature photothermal therapy, Chem. Eng. J. 432 (2022) 134061, https://doi.org/10.1016/j.cej.2021.134061.
[75] Y. Huang, Q. Gao, X. Li, Y. Gao, H. Han, Q. Jin, K. Yao, J. Ji, Ofloxacin loaded MoS2 nanoflakes for synergistic mild-temperature photothermal/antibiotic therapy with reduced drug resistance of bacteria, Nano Res. 13 (9) (2020) 2340–2350, https://doi.org/10.1007/s12274-020-2853-2.
[76] G. Xie, N. Zhou, S. Du, Y. Gao, H. Suo, J. Yang, J. Tao, J. Zhu, L. Zhang, Transparent photothermal hydrogels for wound visualization and accelerated healing, Fundam. Res. 2 (2) (2022) 268–275, https://doi.org/10.1016/j.fmre.2021.10.001.
[77] J. Chen, Y. Liu, G. Cheng, J. Guo, S. Du, J. Qiu, C. Wang, C. Li, X. Yang, T. Chen, Tailored hydrogel delivering niobium carbide boosts ROS-scavenging and antimicrobial activities for diabetic wound healing, Small 18 (27) (2022) 2201300, https://doi.org/10.1002/smll.202201300.
[78] L. Li, X. Sun, M. Dong, H. Zhang, J. Wang, T. Bu, S. Zhao, L. Wang, NIR-regulated dual-functional silica nanoplatform for infected-wound therapy via synergistic sterilization and anti-oxidation, Colloids Surf., B 213 (2022) 112414, https://doi.org/10.1016/j.colsurfb.2022.112414.
[79] W. Duan, X. Liu, J. Zhao, Y. Zheng, J. Wu, Porous silicon carrier endowed with photothermal and therapeutic effects for synergistic wound disinfection, ACS Appl. Mater. Interfaces 14 (43) (2022) 48368–48383, https://doi.org/10.1021/acsami.2c12012.
[80] S. Liu, Z. Liu, M. Wu, X. Xu, F. Huang, L. Zhang, Y. Liu, Q. Shuai, NIR as a “trigger switch” for rapid phase change, on-demand release, and photothermal synergistic antibacterial treatment with chitosan-based temperature-sensitive hydrogel, Int. J. Biol. Macromol. 191 (2021) 344–358, https://doi.org/10.1016/j.ijbiomac.2021.09.093.
[81] L. Feng, Q. Chen, H. Cheng, Q. Yu, W. Zhao, C. Zhao, Dually-thermoresponsive hydrogel with shape adaptability and synergetic bacterial elimination in the full course of wound healing, Adv. Healthcare Mater. 11 (18) (2022) 2201049, https://doi.org/10.1002/adhm.202201049.
[82] W. Wang, D. Ding, K. Zhou, M. Zhang, W. Zhang, F. Yan, N. Cheng, Prussian blue and collagen loaded chitosan nanofibers with NIR-controlled NO release and photothermal activities for wound healing, J. Mater. Sci. Technol. 93 (2021) 17–27, https://doi.org/10.1016/j.jmst.2021.03.037.
[83] X. Chu, Y. Liu, P. Zhang, K. Li, W. Feng, B. Sun, N. Zhou, J. Shen, Silica-supported near-infrared carbon dots and bicarbonate nanoplatform for triple synergistic

sterilization and wound healing promotion therapy, J. Colloid Interface Sci. 608 (2022) 1308–1322, https://doi.org/10.1016/j.jcis.2021.10.147.
[84] X.L. Hu, L. Chu, X. Dong, G.R. Chen, T. Tang, D. Chen, X.P. He, H. Tian, Multivalent glycosheets for double light–driven therapy of multidrug-resistant bacteria on wounds, Adv. Funct. Mater. 29 (14) (2019) 1806986, https://doi.org/10.1002/adfm.201806986.
[85] H. Zhang, Z. Zhang, H. Zhang, C. Chen, D. Zhang, Y. Zhao, Protein-based hybrid responsive microparticles for wound healing, ACS Appl. Mater. Interfaces 13 (16) (2021) 18413–18422, https://doi.org/10.1021/acsami.0c19884.
[86] W.-N. Zeng, D. Wang, Q.-P. Yu, Z.-P. Yu, H.-Y. Wang, C.-Y. Wu, S.-W. Du, X.-Y. Chen, J.-F. Li, Z.-K. Zhou, Y. Zeng, Y. Zhang, Near-infrared light-controllable multifunction mesoporous polydopamine nanocomposites for promoting infected wound healing, ACS Appl. Mater. Interfaces 14 (2) (2022) 2534–2550, https://doi.org/10.1021/acsami.1c19209.
[87] S. Kwiatkowski, B. Knap, D. Przystupski, J. Saczko, E. Kędzierska, K. Knap-Czop, J. Kotlińska, O. Michel, K. Kotowski, J. Kulbacka, Photodynamic therapy – mechanisms, photosensitizers and combinations, Biomed. Pharmacother. 106 (2018) 1098–1107, https://doi.org/10.1016/j.biopha.2018.07.049.
[88] Y. Ren, H. Liu, X. Liu, Y. Zheng, Z. Li, C. Li, K.W.K. Yeung, S. Zhu, Y. Liang, Z. Cui, Photoresponsive materials for antibacterial applications, Cell Rep. Phys. Sci. 1 (11) (2020), https://doi.org/10.1016/j.xcrp.2020.100245.
[89] A. Warrier, N. Mazumder, S. Prabhu, K. Satyamoorthy, T.S. Murali, Photodynamic therapy to control microbial biofilms, Photodiagnosis Photodyn. Ther. 33 (2021) 102090, https://doi.org/10.1016/j.pdpdt.2020.102090.
[90] C. Mao, Y. Xiang, X. Liu, Y. Zheng, K.W.K. Yeung, Z. Cui, X. Yang, Z. Li, Y. Liang, S. Zhu, Local photothermal/photodynamic synergistic therapy by disrupting bacterial membrane to accelerate reactive oxygen species permeation and protein leakage, ACS Appl. Mater. Interfaces 11 (19) (2019) 17902–17914, https://doi.org/10.1021/acsami.9b05787.
[91] S.M. Ayuk, H. Abrahamse, N.N. Houreld, The role of matrix metalloproteinases in diabetic wound healing in relation to photobiomodulation, J. Diabetes Res. 2016 (2016) 1–9, https://doi.org/10.1155/2016/2897656.
[92] M. Migliario, M. Sabbatini, C. Mortellaro, F. Renò, Near infrared low-level laser therapy and cell proliferation: the emerging role of redox sensitive signal transduction pathways, J. Biophot. 11 (11) (2018) e201800025, https://doi.org/10.1002/jbio.201800025.
[93] R.A. Mussttaf, D.F. Jenkins, A.N. Jha, Assessing the impact of low level laser therapy (LLLT) on biological systems: a review, Int. J. Radiat. Biol. 95 (2) (2019) 120–143, https://doi.org/10.1080/09553002.2019.1524944.
[94] A. Yadav, A. Gupta, Noninvasive red and near-infrared wavelength-induced photobiomodulation: promoting impaired cutaneous wound healing, Photodermatol. Photoimmunol. Photomed. 33 (1) (2017) 4–13, https://doi.org/10.1111/phpp.12282.
[95] S.W. Jere, N.N. Houreld, H. Abrahamse, Role of the PI3K/AKT (mTOR and GSK3β) signalling pathway and photobiomodulation in diabetic wound healing, Cytokine Growth Factor Rev. 50 (2019) 52–59, https://doi.org/10.1016/j.cytogfr.2019.03.001.
[96] S. Genah, F. Cialdai, V. Ciccone, E. Sereni, L. Morbidelli, M. Monici, Effect of NIR laser therapy by MLS-MiS source on fibroblast activation by inflammatory cytokines in relation to wound healing, Biomedicines 9 (3) (2021) 307, https://doi.org/10.3390/biomedicines9030307.
[97] G.K. Keshri, A. Gupta, A. Yadav, S.K. Sharma, S.B. Singh, Photobiomodulation with pulsed and continuous wave near-infrared laser (810 nm, Al-Ga-As) augments dermal wound healing in immunosuppressed rats, PLoS One 11 (11) (2016) e0166705, https://doi.org/10.1371/journal.pone.0166705.
[98] G.K. Keshri, G. Kumar, M. Sharma, K. Bora, B. Kumar, A. Gupta, Photobiomodulation effects of pulsed-NIR laser (810 nm) and LED (808±3 nm) with identical treatment regimen on burn wound healing: a quantitative label-free global proteomic approach, J. Photochem. Photobiol., A 6 (2021) 100024, https://doi.org/10.1016/j.jpap.2021.100024.
[99] G.E. Glass, Photobiomodulation: the clinical applications of low-level light therapy, Aesthetic Surg. J. 41 (6) (2021) 723–738, https://doi.org/10.1093/asj/sjab025.
[100] A. Amaroli, S. Ravera, F. Baldini, S. Benedicenti, I. Panfoli, L. Vergani, Photobiomodulation with 808-nm diode laser light promotes wound healing of human endothelial cells through increased reactive oxygen species production stimulating mitochondrial oxidative phosphorylation, Laser Med. Sci. 34 (2019) 495–504, https://doi.org/10.1007/s10103-018-2623-5.
[101] D.H.F.A. Munap, H. Bakhtiar, N. Bidin, G. Krishnan, A. Nabila, N.H. Johari, N. Zakaria, M.A.A. Bakar, P.S. Lau, Wavelength and dose-dependent effects of photobiomodulation therapy on wound healing in rat model, Laser Phys. 28 (11) (2018) 115602, https://doi.org/10.1088/1555-6611/aad84b.
[102] B. Crisan, O. Soritau, M. Baciut, R. Campian, L. Crisan, G. Baciut, Influence of three laser wavelengths on human fibroblasts cell culture, Laser Med. Sci. 28 (2013) 457–463, https://doi.org/10.1007/s10103-012-1084-5.
[103] A. Gupta, T. Dai, M.R. Hamblin, Effect of red and near-infrared wavelengths on low-level laser (light) therapy-induced healing of partial-thickness dermal abrasion in mice, Laser Med. Sci. 29 (2014) 257–265, https://doi.org/10.1007/s10103-013-1319-0.
[104] P. Lau, N. Bidin, G. Krishnan, S.M. AnaybBaleg, M.B.M. Sum, H. Bakhtiar, Z. Nassir, A. Hamid, Photobiostimulation effect on diabetic wound at different power density of near infrared laser, J. Photochem. Photobiol., B 151 (2015) 201–207, https://doi.org/10.1016/j.jphotobiol.2015.08.009.
[105] F. Lovisolo, F. Carton, S. Gino, M. Migliario, F. Renò, Photobiomodulation induces microvesicle release in human keratinocytes: PI3 kinase-dependent pathway role, Laser Med. Sci. (2022) 1–9, https://doi.org/10.1007/s10103-021-03285-2.
[106] C. Mignon, N.E. Uzunbajakava, I. Castellano-Pellicena, N.V. Botchkareva, D. J. Tobin, Differential response of human dermal fibroblast subpopulations to visible and near-infrared light: potential of photobiomodulation for addressing cutaneous conditions, Laser Surg. Med. 50 (8) (2018) 859–882, https://doi.org/10.1002/lsm.22823.
[107] B. Rathnakar, B.S.S. Rao, V. Prabhu, S. Chandra, S. Rai, A.C.K. Rao, M. Sharma, P. K. Gupta, K.K. Mahato, Photo-biomodulatory response of low-power laser irradiation on burn tissue repair in mice, Laser Med. Sci. 31 (2016) 1741–1750, https://doi.org/10.1007/s10103-016-2044-2.
[108] M. Rizzi, M. Migliario, S. Tonello, V. Rocchetti, F. Renò, Photobiomodulation induces in vitro re-epithelialization via nitric oxide production, Laser Med. Sci. 33 (2018) 1003–1008, https://doi.org/10.1007/s10103-018-2443-7.
[109] K.H. Beckmann, G. Meyer-Hamme, S. Schröder, Low level laser therapy for the treatment of diabetic foot ulcers: a critical survey, J. Evidence-Based Complementary Altern. Med. 2014 (2014) 1–9, https://doi.org/10.1155/2014/626127.
[110] Y. Huang, H. Geng, Z. Wu, L. Sun, C. Ji, C.A. Grimes, X. Feng, Q. Cai, An Ag 2 S@ZIF-Van nanosystem for NIR-II imaging of bacterial-induced inflammation and treatment of wound bacterial infection, Biomater. Sci. 10 (14) (2022) 3972–3980, https://doi.org/10.1039/D2BM00550F.
[111] X. Du, W. Wang, C. Wu, B. Jia, W. Li, L. Qiu, P. Jiang, J. Wang, Y.-Q. Li, Enzyme-responsive turn-on nanoprobes for in situ fluorescence imaging and localized photothermal treatment of multidrug-resistant bacterial infections, J. Mater. Chem. B 8 (33) (2020) 7403–7412, https://doi.org/10.1039/D0TB00750A.
[112] J. Lei, S. Rodriguez, M. Jayachandran, E. Solis, K. Epnere, F. Perez-Clavijo, S. Wigley, A. Godavarty, Assessing the healing of venous leg ulcers using a noncontact near-infrared optical imaging approach, Adv. Wound Care 7 (4) (2018) 134–143, https://doi.org/10.1089/wound.2017.0745.
[113] A. Godavarty, Y. Khandavilli, Y. Jung, P.S. Rao, Non-contact optical imaging of healing and non-healing diabetic foot ulcers, in: Optical Biopsy XIII: toward Real-Time Spectroscopic Imaging and Diagnosis, SPIE, 2015, p. 9318, https://doi.org/10.1117/12.2080716.
[114] R. Kwasinski, C. Fernandez, K. Leiva, R. Schutzman, E. Robledo, P. Kallis, L. J. Borda, R. Kirsner, F. Perez-Clavijo, A. Godavarty, Tissue oxygenation changes to assess healing in venous leg ulcers using near-infrared optical imaging, Adv. Wound Care 8 (11) (2019) 565–579, https://doi.org/10.1089/wound.2018.0880.
[115] J.D. Braun, M. Trinidad-Hernandez, D. Perry, D.G. Armstrong, J.L. Mills Sr., Early quantitative evaluation of indocyanine green angiography in patients with critical limb ischemia, J. Vasc. Surg. 57 (5) (2013) 1213–1218, https://doi.org/10.1016/j.jvs.2012.10.113.
[116] S. Li, A.H. Mohamedi, J. Senkowsky, A. Nair, L. Tang, Imaging in chronic wound diagnostics, Adv. Wound Care 9 (5) (2020) 245–263, https://doi.org/10.1089/wound.2019.0967.
[117] M.G. Sowa, W.-C. Kuo, A.C. Ko, D.G. Armstrong, Review of near-infrared methods for wound assessment, J. Biomed. Opt. 21 (9) (2016), https://doi.org/10.1117/1.JBO.21.9.091304, 091304-091304.
[118] J. Shin Chin, L. Madden, S. Yian Chew, A.R. Phillips, D.L. Becker, Wound healing and its imaging, Imaging Technol. Transdermal Delivery Skin Disord. (2019) 15–34, https://doi.org/10.1002/9783527814633.ch2.
[119] C. Yang, C. Yang, Y. Chen, J. Liu, Z. Liu, H.-J. Chen, The Trends in wound management: sensing, therapeutic treatment, and “theranostics”, J. Sci.: Adv. Mater. Devices. 8 (4) (2023) 100619 https://doi.org/10.1016/j.jsamd.2023.100619.
[120] Y. Yang, K. Huang, M. Wang, Q. Wang, H. Chang, Y. Liang, Q. Wang, J. Zhao, T. Tang, S. Yang, Ubiquitination flow repressors: enhancing wound healing of infectious diabetic ulcers through stabilization of polyubiquitinated hypoxia-inducible factor-1α by theranostic nitric oxide nanogenerators, Adv. Mater. 33 (45) (2021) 2103593, https://doi.org/10.1002/adma.202103593.
[121] P. Ran, H. Zheng, W. Cao, X. Jia, G. Zhang, Y. Liu, X. Li, On-demand changeable theranostic hydrogels and visual imaging-guided antibacterial photodynamic therapy to promote wound healing, ACS Appl. Mater. Interfaces 14 (43) (2022) 49375–49388, https://doi.org/10.1021/acsami.2c15561.
[122] Z. Mei, D. Gao, D. Hu, H. Zhou, T. Ma, L. Huang, X. Liu, R. Zheng, H. Zheng, P. Zhao, Activatable NIR-II photoacoustic imaging and photochemical synergistic therapy of MRSA infections using miniature Au/Ag nanorods, Biomaterials 251 (2020) 120092, https://doi.org/10.1016/j.biomaterials.2020.120092.
[123] R.P. Morais, S. Hochheim, C.C. de Oliveira, I.C. Riegel-Vidotti, C.E. Marino, Skin interaction, permeation, and toxicity of silica nanoparticles: challenges and recent therapeutic and cosmetic advances, Int. J. Pharm. 614 (2022) 121439, https://doi.org/10.1016/j.ijpharm.2021.121439.
[124] M.I. Hossain, S.S. Nanda, S.T. Selvan, D.K. Yi, Recent insights into NIR-light-responsive materials for photothermal cell treatments, Nanomaterials 12 (19) (2022) 3318, https://doi.org/10.3390/nano12193318.
[125] D. Jaque, L.M. Maestro, B. del Rosal, P. Haro-Gonzalez, A. Benayas, J. Plaza, E. M. Rodríguez, J.G. Solé, Nanoparticles for photothermal therapies, Nanoscale 6 (16) (2014) 9494–9530, https://doi.org/10.1039/C4NR00708E.
[126] B. Li, Y. Zhang, R. Zou, Q. Wang, B. Zhang, L. An, F. Yin, Y. Hua, J. Hu, Self-assembled WO 3− x hierarchical nanostructures for photothermal therapy with a 915 nm laser rather than the common 980 nm laser, Dalton Trans. 43 (16) (2014) 6244–6250, https://doi.org/10.1039/C3DT53396D.
[127] P. Zhang, M.X. Wu, A clinical review of phototherapy for psoriasis, Laser Med. Sci. 33 (2018) 173–180, https://doi.org/10.1007/s10103-017-2360-1.
[128] R. Zhang, Z. Zhang, J. Han, L. Yang, J. Li, Z. Song, T. Wang, J. Zhu, Advanced liquid crystal-based switchable optical devices for light protection applications: principles and strategies, Light Sci. Appl. 12 (1) (2023) 11, https://doi.org/10.1038/s41377-022-01032-y.

[129] P. Youssef, N. Sheibani, D. Albert, Retinal light toxicity, Eye 25 (1) (2011) 1–14, https://doi.org/10.1038/eye.2010.149.
[130] A. Capon, G. Iarmarcovai, D. Gonnelli, N. Degardin, G. Magalon, S. Mordon, Scar prevention using laser-assisted skin healing (LASH) in plastic surgery, Aesthetic Plast. Surg. 34 (2010) 438–446, https://doi.org/10.1007/s00266-009-9469-y.
[131] R.L.d.P. Carvalho, P.S. Alcântara, F. Kamamoto, M.D.C. Cressoni, R.A. Casarotto, Effects of low-level laser therapy on pain and scar formation after inguinal herniation surgery: a randomized controlled single-blind study, Photomed. Laser Surg. 28 (3) (2010) 417–422, https://doi.org/10.1089/pho.2009.2548.
[132] A. Haze, L. Gavish, O. Elishoov, D. Shorka, T. Tsohar, Y.N. Gellman, M. Liebergall, Treatment of diabetic foot ulcers in a frail population with severe co-morbidities using at-home photobiomodulation laser therapy: a double-blind, randomized, sham-controlled pilot clinical study, Laser Med. Sci. 37 (2) (2022) 919–928, https://doi.org/10.1007/s10103-021-03335-9.
[133] P. Longobardi, V. Hartwig, L. Santarella, K. Hoxha, J. Campos, M. Laurino, P. Salvo, M.G. Trivella, F. Coceani, M. Rocco, Potential markers of healing from near infrared spectroscopy imaging of venous leg ulcer. A randomized controlled clinical trial comparing conventional with hyperbaric oxygen treatment, Wound Repair Regen. 28 (6) (2020) 856–866, https://doi.org/10.1111/wrr.12853.